Helmholtz-Zentrum Dresden-Rossendorf (HZDR)

HELMHOLTZ ZENTRUM
DRESDEN ROSSENDORF

Impact of low energy ion beams on the properties of rr-P3HT films

Kislyuk, V.; Kotrechko, S.; Trachevskij, V.; Melnyk, A.; Pud, A.; Ogurtsov, N.; Noskov, Y.; Osiponok, M.; Lytvyn, P.; Dzyazko, Y.; Nierobisch, F.; Schneider, A.; Ludewig, F.; Akhmadaliev, S.; Aniol, R.; Kentsch, U.; Krause, M.; Facsko, S.;

Originally published:

September 2020

Applied Surface Science 535(2020), 147619

DOI: https://doi.org/10.1016/j.apsusc.2020.147619

Perma-Link to Publication Repository of HZDR:

https://www.hzdr.de/publications/Publ-30504

Release of the secondary publication
on the basis of the German Copyright Law § 38 Section 4.

CC BY-NC-ND

Applied Surface Science

Impact of low energy ion beams on the properties of rr-P3HT films

--Manuscript Draft--

Manuscript Number:	APSUSC-D-20-03092R2
Article Type:	VSI: SURFINT-SREN VI
Keywords:	ion implantation, rr-P3HT, doping, resistance, ac impedance, organic electronics
Corresponding Author:	Victor V. Kislyuk, Ph.D. Institut metalofiziki imeni G V Kurdumova Nacional'na akademia nauk Ukraini Kyiv, UKRAINE
First Author:	Victor V. Kislyuk, Ph.D.
Order of Authors:	Victor V. Kislyuk, Ph.D.
	Sergiy O Kotrechko, Professor
	Volodymyr V Trachevskij, Ph.D.
	Andrii K Melnyk
	Alexander A Pud, Professor
	Nikolay A Ogurtsov, Ph.D.
	Yuriy V Noskov, Ph.D.
	Mykola M Osiponok
	Peter M Lytvyn, Ph.D.
	Yulia S Dzyazko, Dr.
	Shavkat Akhmadaliev, Dr.
	Ulrich Kentsch, Dr.
	Matthias Krause, Dr.
	Stefan Facsko, Dr.
Abstract:	Two types of ions (fluorine and titanium) are implanted into the film of regio-regular poly(3-hexylthiophene-2,5-diyl) (rr-P3HT) spin-coated on a glass substrate with subsequent annealing in argon atmosphere to modify their electrical properties and structure. The ion energy and fluence were within 0.2 keV - 40 keV and 10^13 - 10^15 cm^-2 respectively. The dc resistance enhances after the intensive ion beam treatment while the ac impedance decreases. Ti ion implantation with 40 keV energy and 10^14 cm^-2 fluence induces decrease of the ac impedance by almost two orders of magnitude and appearance of the molecular hydrogen features in 1H NMR spectrum. The UV-VIS spectra of the films are blue shifted after their exposal to the ion beams, which correlates with the presence oxygen. The ratio of the oxygen to carbon peak intensities (ξ=O1s/C1s) in the XPS spectra is proposed as a measure for the local partial disturbance of the film. EPR spectra demonstrate formation of the paramagnetic states with g factor less than 2, which is accompanied with the down-field shift of the NMR spectrum. The ion beams are found to make no etching effect as per results of the film thickness measurements and AFM images.

Powered by Editorial Manager® and ProduXion Manager® from Aries Systems Corporation

Highlights

- Low energy ion beams can control rr-P3HT properties for flexible electronics.
- UV-VIS absorption spectra of rr-P3HT are blue shifted after ion beam treatment.
- EPR and NMR reveal polaronic states induced in the polymer after ion implantation.
- XPS 1s oxygen peak indicates the ion beam-induced disturbances of the film.
- The ion implantation causes decrease of ac impedance.

Manuscript Click here to view linked References

Impact of low energy ion beams on the properties of rr-P3HT films

Victor Kislyuk[1,2*], Sergiy Kotrechko[1], Volodymyr Trachevskij[3], Andrii Melnyk[4], Alexander Pud[5], Nikolay Ogurtsov[5], Yuriy Noskov[5], Mykola Osiponok[6], Peter Lytvyn[6], Yulia Dzyazko[7], Shavkat Akhmadaliev[8], Ulrich Kentsch[8], Matthias Krause[8], Stefan Facsko[8]

[1]G. V. Kurdyumov Institute for Metal Physics, NAS of Ukraine,
36 Academician Vernadsky Boulevard, UA-03142 Kyiv, Ukraine
[2]National Aviation University, Kosmonavta Komarova Ave. 1, Kyiv, Ukraine
[3]Technological Center, NAS of Ukraine, Pokrovska str. 13, 04070 Kyiv, Ukraine
[4]Institute for Sorption and Problems of Endoecology, NAS of Ukraine, Naumov str. 13,03028 Kyiv, Ukraine
[5] V. P. Kukhar Institute of Bioorganic Chemistry and Petrochemistry, NAS of Ukraine,
50 Kharkivske shose,02160, Kyiv, Ukraine
[6]V. E. Lashkaryov Institute of Semiconductor Physics, NAS of Ukraine, pr. Nauky 45, 03028 Kyiv, Ukraine
[7] V. I. Vernadskiy Institute of General and Inorganic Chemistry, NAS of Ukraine,
Palladin Ave. 32 - 34, 03680 Kyiv, Ukraine.
[8]Institute of Ion Beam Physics and Mat. Res., Helmholtz-Zentrum Dresden-Rossendorf e.V.,
01314 Dresden, Germany.
**Contact person, e-mail: E- mail: viktor.kislyuk@gmail.com*

Two types of ions (fluorine and titanium) are implanted into the film of regio-regular poly(3-hexylthiophene-2,5-diyl) (rr-P3HT) spin-coated on a glass substrate with subsequent annealing in argon atmosphere to modify their electrical properties and structure. The ion energy and fluence were within 0.2 keV – 40 keV and 10^{13} – 10^{15} cm^{-2} respectively. The dc resistance enhances after the intensive ion beam treatment while the ac impedance decreases. Ti ion implantation with 40 keV energy and 10^{14} cm^{-2} fluence induces decrease of the ac impedance by almost two orders of magnitude and appearance of the molecular hydrogen features in ^{1}H NMR spectrum. The UV-VIS spectra of the films are blue shifted after their exposal to the ion beams, which correlates with the presence of oxygen. The ratio of the oxygen to carbon peak intensities (ξ =O1s/C1s) in the XPS spectra is proposed as a measure for the local partial disturbance of the film. EPR spectra demonstrate formation of the paramagnetic states with g factor less than 2, which is accompanied with the down-field shift of the NMR spectrum. The ion beams are found to have no significant etching effect as per results of the film thickness measurements and AFM images.

Key words: ion implantation, rr-P3HT, doping, resistance, ac impedance, organic electronics.

1. Introduction

rr-P3HT based active layers are often applied as constituents of organic electronics devices, in particular, organic photovoltaic cells (OPVs) [1–4], organic field effect transistors (OFETs) [5,6], electrochromic devices [7] and thermoelectric converters [8]. The long conjugated polymer chain is responsible for their semiconducting properties: i) electron conductivity (and electrical

parameters like resistance and ac impedance associated herewith) and possibility to control it via doping (incorporation of elements inducing conducting electron states called polarons and bipolarons [9,10]); ii) relatively narrow HOMO-LUMO gap (with optical absorption spectrum being within the visible light, which makes this material promising for photocatalysis, particularly, for photocatalytic water splitting [11]).

Light weight and rather low cost of the production make the films of rr-P3HT to be attractive for flexible electronics which becomes a demanding field not only for research but also for commerce [12,13]. The key requirements for such an application are the technological compatibility (applicability of some chemicals, doping methods, temperature conditions) with flexible substrates, as well as elasticity of the films themselves. The latter is rather a severe restriction since the regio-regularity of these films envisages some fragility as it is a comb-like structure ordered in rather rigid frame of polymer molecules [14,15]. It is, actually, the system of percolation paths which is a crucial platform for electron transport. Thus, there are two mutually contradictory demands of low electrical resistivity and elasticity, which is a challenge for trade-offs between their electrical and mechanical properties [16]. Meanwhile, the films of the conducting polymers are rather appropriate for flexible applications as the methods of their fabrication do not need processes capable to destroy the substrate material. The most applicable process to control the electrical properties of the organic semiconductors is molecular doping [17,18] where a dopant is added through the whole volume of the film or even prior to their placing to a substrate. Electronic circuits of more complex functionality include local conducting regions, and ion implantation is a technique widely used in conventional electronics for producing the local doping. This approach is compatible also with flexible electronic requirements such as low temperature of the process and possibility to apply reduced energies of the ions (in particular for the case of plasma-based mode of the ion beam formation [19]). There are several mechanisms known for the ion beam-induced resistivity reduction in organic conjugated polymers. The doping itself is found to be of minor importance, whereas the principal constituent of the resistivity decrease originates from the carbonization, i.e. hydrogen debonding with formation of carbon-rich fragments [20,21]. The role of the ion beam in this case relates to the destructing ability of an ion [22] (ion beam energy, ion mass and radius) rather than to its chemical activity. The ion energy and mass determine also the ion stopping mechanisms: dominantly electron or nuclear stopping for light or fast and heavy or slow ions, respectively [23].

On the other hand, the implantation of metal ions is found to be able to produce metal nanoclusters inside the film [24]. Hence, the formation of percolation paths of conducting nanoclusters is quite possible after the implantation of metal ions.

The objective of this research is to study the possibility for the ion implantation technique (widely used in conventional electronics for production of integrated circuits with high functionality) to modify the organic rr-P3HT film properties crucial for their functionality as electronic components. Despite the great potential of this technique, there are very few studies regarding its application to organic flexible electronic components. The data available in this field represent *a priory* rather wide spectrum of the above mechanisms responsible for the electron structure modifications induced by various ion beams in an organic polymer film. To clarify the role of each mechanism, its origin and conditions when it is revealed is a task of high importance as far as it concerns the methods to control the process. For this reason, two distinct types of ions were chosen F^+ and Ti^+ which distinguished drastically by the following parameters: i) weight (light F^+ and heavy Ti^+) affecting the stopping range R_p, the mechanical momentum and local disturbance of the polymer morphology; ii) reactivity defined by electronegativity responsible for doping effect producing polaronic states; iii) metal (titanium) and nonmetal (fluorine) to monitor for metallic clusters forming additional channels for the electric current flow.

2. Experimental part

Briefly, the experiment consists of three parts: fabrication of a set of samples (rr-P3HT films spin-coated on glass substrate and treated in a due course), exposal of the samples with ion beams of Ti^+ and F^+ (each sample with its own specific parameters of the treatment described in table 1), and measurement of the properties of the samples.

2.1. Fabrication of the rr-P3HT samples

The 25mm x 25mm x 1mm glass substrates (cut from microscope slides of soda lime glass, Paul Marienfeld GmbH & Co.KG, Germany) were ultrasonicated in acetone (3 min) and isopropanol (3 min), then rinsed by distilled water followed by 5 min treatment in boiling 35 wt.% hydrogen peroxide water solution; then again rinsed by distilled water and finally dried at ~60 ^oC.

20 microliters of 2 wt% solutions of regioregular poly(3-hexylthiophene-2,5-diyl) (Rieke Metals, Item # 4002-E, 90%-93% regioregularity) in chlorobenzene were dropped on the freshly cleaned glass substrates and then spin-coated at 2000 rpm for 20 s. Finally, the samples coated with formed thin rr-P3HT films were annealed at 120 ^oC for 30 min under argon.

Four indium contacts were deposited onto the top of the films through the mask for electrical transport measurements (Fig. 1, inset). The mask enables the identical configuration of the contacts. The planar geometry of the terminals enables monitoring even thin near-surface layer, which is of particular importance for the ions with low energy and shorter penetration depth correspondently. The terminal areas were located at a film periphery to avoid screening both for

ion incidence and optical beam (while optical absorbance measurements). Thus, this contact configuration allowed us to control electrical and optical features of the same area of the film after its treatment with an ion beam.

The samples intended for NMR and EPR measurements were cut into strips of 3 mm wide and packed into the ampoule.

2.2. Ion implantation

The samples were irradiated with Ti^+ and F^+ ions of 0.2, 1, 10 and 40 keV energies. The choice of energy range was based on the preliminary modelling with standard software of Stopping and Range of Ions in Matter (SRIM). The stopping ranges R_p were simulated for the rr-P3HT material with stoichiometric formula of $C_{10}H_{14}S$ and 1.3 g/cm^3 density. The criterion of the appropriate energy value was the R_p magnitude predetermined by the film thickness.

The values of the fluences were 10^{13}, 10^{14}, 10^{15} cm^{-2}. The conditions used for various samples are described in table 1. SF_6 gas was used as a source for fluorine ions. The starting vacuum was within the range of $5x10^{-8} – 2x10^{-6}$ mbar. The sample holders were cooled to keep the room temperature during the whole processing. The ion current was kept at 0.033 – 0.066 μA for lower fluencies and 0.5 – 0.66 μA for higher fluencies. To check the influence of the current on the local conditions of the films, the additional measurements were conducted on the samples treated by ions with various current values from the above range. No differences were found in the UV-VIS spectra of these samples. One sample was left as it was prepared without implantation and used then as reference sample (it is marked as Ref in table 1).

2.3. Measurement of the film properties.

UV-VIS absorption spectra were calculated from data on the film transmission registered with a grating spectrometer. As a reference were used a bare glass substrate identical to those used as substrates for the film spin-coating and pristine samples of rr-P3HT covered glass. The spectra were measured for each sample prior and after implantation. The initial spectrum of each pristine sample was used for the calculation of the reduced spectrum of the same sample after implantation to compare spectra for the same sample before and after the ion treatment. The UV-VIS absorption spectra of the exposed samples were calculated as a reduced optical density function:

$$f_{O.D.}(\lambda) = \frac{\ln\left(\frac{I_0(\lambda)}{I(\lambda)}\right)}{\left[\ln\left(\frac{I_0(\lambda)}{I_b(\lambda)}\right)\right]_{max}} \quad , \qquad (1)$$

where $I_0(\lambda)$, $I(\lambda)$ and $I_b(\lambda)$ are intensities of the optical beam with λ wavelength transmitted through bare glass substrate, glass substrate with the rr-P3HT film and the same film before the ion treatment, respectively. The spectra are reduced to the maxima of the initial spectra (the expression in the denominator). Thus, the spectra of the samples before the exposal have unity value at the maximum, and the changes induced by the ion beams in the absorption are represented as to the initial spectrum.

XPS spectra were taken at room temperature with a Microlab 310 system (with a base pressure of 6x10-10 mbar) by Thermo Fisher Scientific using the nonmonochromized Mg Kα line of a dual-anode X-ray source. The X-ray angle of incidence was 30° and the spectrometer entrance at 0° with respect to the surface normal. The values of relative sensitivity factors (R.S.F.) are taken from internal XPS sensitivity factor database of the Thermo Fisher Program Avantage version 3.79.

DC resistance was measured by Keysight Technologies B2900A Series Precision Source/Measure Unit in 4-probe circuit both in constant current and constant voltage modes. The source output was connected to 1-2 terminals (Fig.1, inset), and the resistance (R) was derived as:

$$R = \frac{V_{3-4}}{I}, \tag{2}$$

where V_{3-4} is the voltage between the terminals 3 and 4, I is the current value in the circuit 1-2. The resistance is reversely proportional to the film conductivity (σ):

$$R \sim 1/\sigma, \tag{3}$$

and, thus, its value reflects the electrical properties of the film at the direct current (dc) mode. The lower value of the resistance the better conditions for the direct current flow, as the current is in denominator (1).

AC impedance spectrometer (AUTOLAB) was connected to terminals 3-4 (Fig.1, inset). The real and imaginary parts of the impedance were measured as frequency was swept within 10 MHz – 10 mHz. Nyquist diagrams were plotted on the basis of the values measured at various frequencies. The impedance (Z) monitors electrical properties at alternating current (ac) mode. This is complex quantity consisting of real (**Re**{Z}) and imaginary (**Im**{Z}) parts reflecting both the ability to hamper the current flow and the phase shift between the source output and the sample response. The ac impedance allows one to register conducting species even when they are separated enough to prevent current flow in dc mode. The total impedance value:

$$|Z| = \sqrt{\mathbf{Re}\{Z\}^2 + \mathbf{Im}\{Z\}^2} \quad (4)$$

depends on the conductivity of the contributing constituent species. Briefly, a lower impedance value corresponds to either higher conductivity of the individual conducting species or a larger quantity of them, whereas the dc resistance relates to those of them which are electrically connected (in the sense of the dc mode) and form a net of continuous percolating paths for the dc current flow. Thus, dc resistance and ac impedance are complementary techniques for better understanding the electrical behavior of a substance.

EPR were recorded on a X-band spectrometer Bruker Elexsys E580 at room temperature (295 K). The resonator was tuned for each ampoule individually (the preparation of the samples is described in 2.1 paragraph). Sample of diphenylpicrylhydrazyl (DPPH) with g = 2,0036 was used for the spectrometer calibration.

NMR spectra were registered by NMR spectrometer Bruker Avance 400 (9.4 T magnetic field) at frequency 400.130 MHz (^{1}H). The signal was accumulated after electromagnetic pulses of 6 – 10 μs duration repeated with 0.5 – 4 s period of time. Chemical shift (δ, ppm) was determined as to the reference spectrum of tetramethylsilane.

AFM height maps (images) of selected samples were collected by the NanoScope IIIa Dimension 3000^{TM} scanning probe microscope, operated in tapping mode. Commonly used silicon probes of 10 nm nominal tip apex radius were applied.

Bruker **Dektak** profiler was used for the film thickness measurements. The films were scratched through the whole depth till glass substrate. The tip was scanned perpendicularly to the groove, and the hill and valley values at the profile were averaged to get the difference corresponding to the depth value.

Table 1. The sample list with description of the ion beam treatment. Parameters of ξ =O1s/C1s, $\xi_{at} = \xi \cdot S_{C1s}/S_{O1s}$, where O1s, C1s, S_{C1s}/S_{O1s} =1/2.93 are intensities of XPS signals for 1s electrons of oxygen and carbon and ratio of their R.S.F., respectively.

No.	Sample Code	Ion type	Energy, eV	Fluence, cm^{-2}	ξ	ξ_{at}, %
1	Ref	Pristine sample	-	-	0.06	2.0
2	F02_13	F^+	0.2	10^{13}	0.16	5.5
3	F02_14	F^+	0.2	10^{14}	0.26	8.9
4	F02_15	F^+	0.2	10^{15}	0.71	24.2
5	F1_13	F^+	1	10^{13}	0.26	8.9
6	F1_14	F^+	1	10^{14}	0.33	11.3
7	F1_15	F^+	1	10^{15}	0.74	25.3
8	F10_13	F^+	10	10^{13}	0.12	4.1
9	F10_14	F^+	10	10^{14}	0.43	14.7
10	F10_15	F^+	10	10^{15}	-	-
11	F40_13	F^+	40	10^{13}	0.14	4.8
12	F40_14	F^+	40	10^{14}	0.51	17.4
13	Ti02_13	Ti^+	0.2	10^{13}	0.15	5.1
14	Ti02_14	Ti^+	0.2	10^{14}	0.36	12.3
15	Ti02_15	Ti^+	0.2	10^{15}	1.57	53.6
16	Ti1_13	Ti^+	1	10^{13}	0.18	6.1
17	Ti1_14	Ti^+	1	10^{14}	0.33	11.3
18	Ti10_13	Ti^+	10	10^{13}	0.17	5.8
19	Ti10_14	Ti^+	10	10^{14}	0.45	15.4
20	Ti40_13	Ti^+	40	10^{13}	0.14	4.8
21	Ti40_14	Ti^+	40	10^{14}	0.67	22.9

3. Results and discussions

3.1. DC resistance and UV-VIS absorption

The samples are initially of high resistance within 20 – 40 GOhm range. The shaded area in Fig. 1 is a schematic representation of the resistance range measured for the pristine samples. The samples treated with ion beams of relatively low fluence of 10^{13}cm^{-2} with energy of 0.2 and 1 keV have lower values of the resistance. The profiles of their absorption spectra (curves 1 – 7, Fig.2a) remain the same as those of the initial samples before the treatment, while the integral intensity decreases. The samples after the fluence of 10^{15}cm^{-2} have substantially higher resistance, for instance, the treatment with ions of 0.2 keV energy gives rise to complete loss of the connectivity at high fluencies (depicted schematically as lines directed to infinity in Fig.1). Similar behavior of the resistance is found after ion implantation of 40 keV energies regardless of fluence from the range in question (is not depicted in Fig.1). The resistance enhancement is accompanied by the bleaching of the samples with the blue-shift of the UV-VIS absorption spectra (Fig. 2) after ion implantation with 10^{15} см$^{-2}$ fluence (curves 16, 17 and 18) or with 40 keV energy (curves 12 – 15). This behavior is in consistence with the non-monotonous dependence of dc conductivity (the quantity reversely proportional to the resistance) on the fluence reported for samples irradiated with γ-rays and e-beams [25]. Our experiments demonstrate similar impact of the ion treatment on the resistance regardless of the ion nature. The main reason is the scission of the polymer bonds which yields shorter molecular fragments of the conjugation chain. The blue shift of the UV-VIS absorption points to the same inference since the shorter conjugation length the wider HOMO-LUMO gap [26,27].

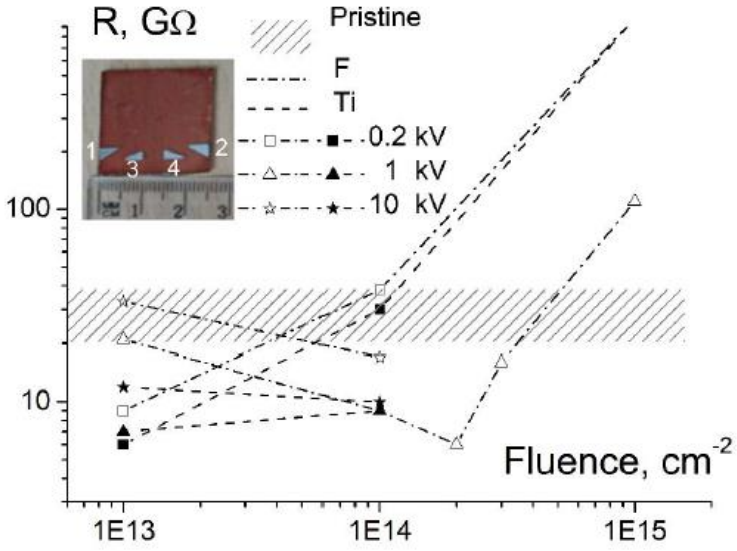

Fig. 1. The sample resistance measured from 4-probe circuit versus fluence of the respective ion beam. **Inset.** Photo of a sample with contacts. The contact numbers correspond to the following connections: 1,2 – power supply; 3,4 – voltmeter (top view).

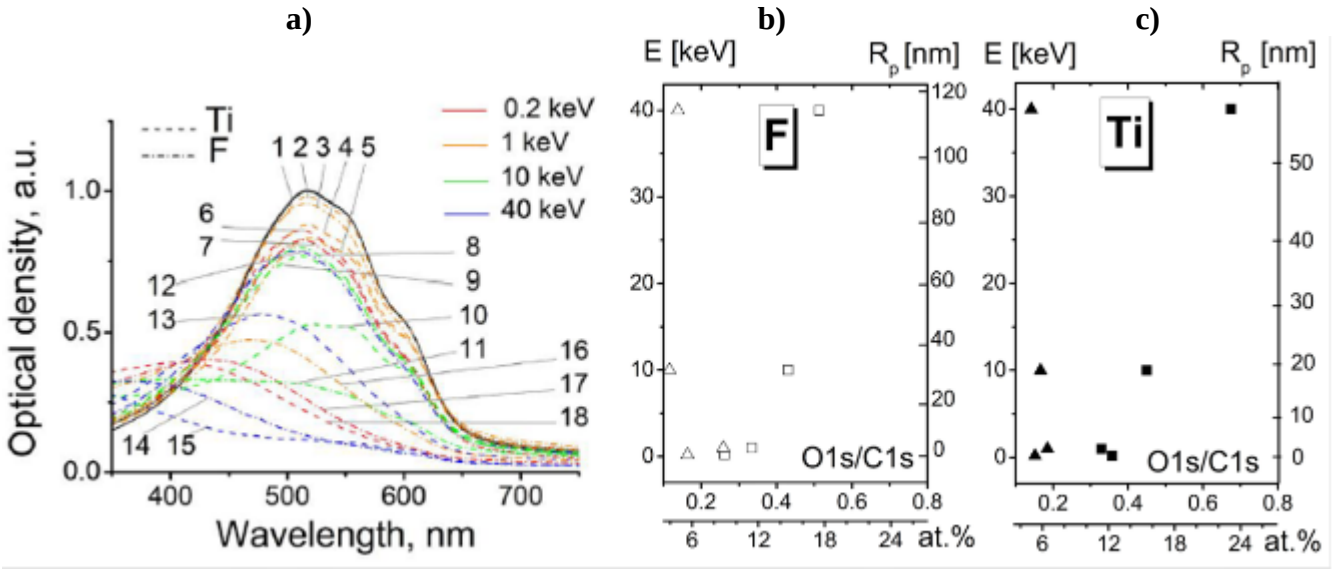

Fig.2. a) UV-VIS absorption spectra of the rr-P3HT samples: 1 – Ref, F02_13, Ti02_13; 2 – Ti1_13; 3 – F1_13; 4 – Ti1_14; 5 – F1_14; 6 – Ti02_14; 7 – F02_14; 8 – F10_13; 9 – Ti10_13; 10 – Ti10_14; 11 – F10_14; 12 – F40_13; 13 – Ti40_13; 14 – F40_14; 15 – Ti40_14; 16 – F1_15; 17 – F02_15; 18 – Ti02_15. b,c) dependencies which relate ion energy in keV, the stopping range projection R_p in nm (calculated in SRIM software) and ratio of the 1s XPS peak intensities of oxygen and carbon O1s/C1s for samples treated by ions of F (b) and Ti (c) for two values of fluence: 10^{13} cm^{-2} (Δ,▲) and 10^{14} cm^{-2} (□,■); additional bottom axes represent O1s/C1s in at.%.

Thus, there are two distinct types of the film response to the ion beam treatment (depending on the energy and fluence). **Type 1** corresponds to low values of energy (0.2, 1 keV) provided the fluence values are also low (10^{13}, 10^{14} cm^{-2}). The behavior of this type is characterized by decrease of the spectrum intensity as whole, while the spectral profile remains unchanged (Fig. 2a, curves 1 – 7). The resistance of the sample either remains the same or even slightly decreases. **Type 2** contains all the rest cases considered in this research, i.e. higher energies (10 and 40 keV) or the highest fluence (10^{15} cm^{-2}) with low energies. The spectra become blue shifted, with resistance increasing by several orders of magnitude.

The principle difference between these two modes is apparently the depth of the volume disturbed by the ion beams. The latter is determined by R_p parameter which is lower for lower energies (Fig. 2, b,c). This parameter depends also on the type of ion: the stopping rate is longer for lighter ions. The blue shift for the samples of type 2 is indicative of the scission effect induced by the disturbance through the whole thickness of the film. The similar effect is likely realized in the samples of type 1, but the depth of the disturbed volume is shorter, and both disturbed and undisturbed layers contribute to the overall spectrum. A slight increase of the short wavelength edge with total intensity decrease of the intrinsic absorption argues for the favor of the above assumption. Although the surface roughness modified via the ion beam incidence might impact on the absorption intensity, its role seems to be minor. Actually, the roughness governs mainly

either reflection or scattering of the incident light. Hypothetically each of them can affect the denominator $I(\lambda)$ (in equation 1) representing the intensity of the transmitted light. The roughness increase (in short and very schematic interpretation) reduces the reflectance and enhances scattering. Thus, the final impacts of these factors have opposite signs, and their influences are mutually compensated.

3.2. AC impedance

Fig.3 demonstrates the results on the ac impedance measurements presented as Nyquist diagrams (Z´´=**Im**{Z} vs Z´=**Re**{Z}) in three various ranges of the real and imaginary part. In general, the impedance registered at the planar contact terminals tends to decrease after the ion beam treatment. However, the dependence of the impedance on fluence or energy is not distinct. For instance, Ti^+ ions of 0.2 keV energy induce the impedance increase with increasing the fluence from 10^{14} to 10^{15} cm^{-2}, while F^+ ions of the same energy cause the impedance reduction within the same fluence range. The impedance value is lower than that of the pristine sample for both cases. The comparison of the impacts made by the ions of different nature and the same energies of 0.2 and 1 keV reveals that fluorine ions make stronger impact on the decrease of the ac impedance than titanium ions do. This is attributed to different stopping depth. The ions of such low energies act generally at the near surface region due to the penetration depth of several nm (while the film thickness is ~40 – 70 nm). It is the depth that is monitored by the planar contacts 3-4 on the film surface (Fig.1, inset photo) while ac impedance measurements. Since ac impedance reduces while the dc resistance increases after the same processing of ion treatment with 0.2 keV energy, the ions not only destroy the percolation paths responsible for the dc resistance but also produce new factors favorable for improving ac current flow. Firstly, this means that adjacent fragments of the former (before ion intrusion) integral conjugated chain keep, at least, capacitive coupling. Secondly, ions cause doping of these fragments (details on the possible mechanism of doping and its polaronic nature is considered in 3.4 paragraph). Fig.3d illustrates schematically the equivalent circuit explaining these two consequences of an ion beam incidence onto the conductive fragment of the percolation path. Initially this fragment has resistance R_I. The action of the ion is twofold: it incorporates into the conducting channel disconnecting it via splitting into two constituents and it creates conditions for additional doping of these split residuals remaining at the vicinity of each other. Thus, the dc percolation is disconnected whilst the capacitive coupling forms between these adjacent parts with lower impedance value due to the doping effect of the interlayer depicted as a capacitor in Fig.3d.

Thirdly, upper layers subjected to strong destruction (as for the case of low energy and high fluence) lose the ability to conduct electricity both in dc and ac mode. The latter takes place, particularly, for the case of titanium ions. Their projected stopping range R_p is shorter than that of fluorine ions (Fig.2, b and c, right axis), while Ti ions have stronger momentum capable of harder destruction of the near surface layers. This is the reason that impedance of Ti02_15 (Fig.3a) sample higher substantially (approximately by factor of 5) than that of F02_15 (Fig.3b).

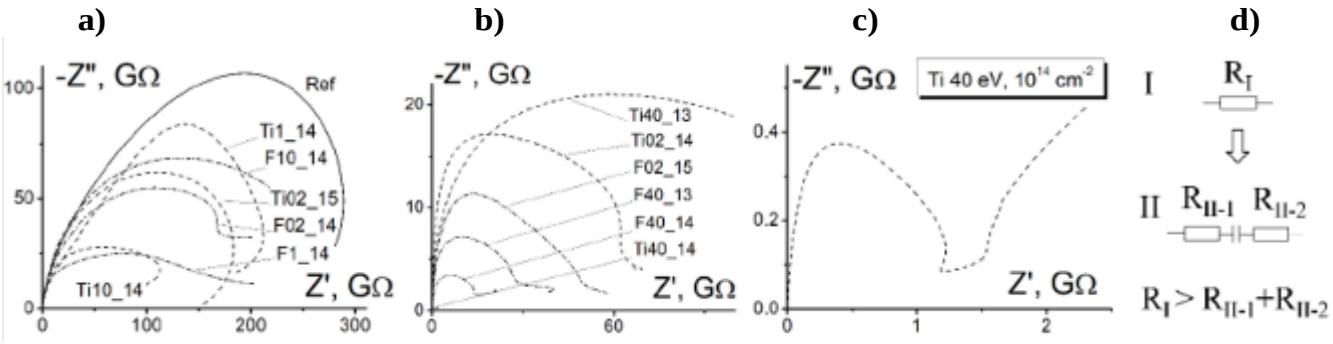

Fig. 3. a), b), c): Nyquist diagrams plotted on the basis of ac impedance spectroscopy data; **d)** schematic representation of the equivalent circuit for the fragment subjected to the ion beam: I – before and II – after the ion incidence.

Ions of higher energies of 10 and 40 keV are revealed to cause decrease of ac impedance, with titanium ions making stronger impact than fluorine ions. The ac impedance monotonously decreases with fluence change from 10^{13} to 10^{14} cm^{-2} for both types of ions with 40 keV energy (Fig. 3b). The value of R_p for titanium ions is almost two times as low as that for fluorine ions for 10 – 40 keV range (Fig.2, b and c). Thus, the beam of titanium ions treats the region closer to the contacts where the ac impedance spectrometer is connected. In addition, the higher energy the higher momentum with its value reaching magnitude sufficient to drive some individual nanocrystallites. The structure of the P3HT nanocrystallites is a result of the spin coating followed by the appropriate annealing [28,29]. The nanocrystallites form ordered net of percolating paths contributing to the overall current flow. Since the film is formed under the transitional conditions enforced by the substrate (details are in 3.4 paragraph) the structure itself is not optimal for the electron transport. The ions of sufficient momentum correct the mutual position of the crystallites packing them into a configuration increasing the number of the percolation paths. Titanium ions have advantages due to their mass and thus stronger momentum. Additionally, Ti atoms agglomerate into fine nanospecies ordered into alternative nets of dispersed conducting nanoislands. The value of impedance for Ti40_14 sample is by circa 2 orders of magnitude lower than that of the pristine sample (Fig. 3c). Nyquist curve for this sample consists of two constituents revealed at various frequencies: high frequency component relates to the conductivity along the individual polymer fragments; low frequency component is a consequence

of the appearance of the alternative path for the ac flow through the system of titanium nanospecies which can diffuse contributing to the low frequency component of the ac impedance.

3.3. XPS and UV-VIS absorption.

XPS spectra of the samples after treatment under F^+ or Ti^+ beams contain peaks corresponding to fluorine or titanium, respectively, only for 0.2 keV energy and 10^{15} cm^{-2} fluence (Fig. 4a, curves 10 and 11). F1s peak is almost two times as weak as Ti2p, which agrees with the ratio of their sensitivity factors. The survey spectra of the samples after treatments with the fluency of 10^{15} cm^{-2} and 0.2 keV energy contain features of a corresponding implanting ion. The stopping range for this energy is close to X-ray penetration depth of 0.3 – 4 nm [30].

The comparison of UV-VIS (Fig. 2a) and XPS (Fig. 4a) spectra demonstrates the correlation between the changes in the absorption spectra (particularly, their spectral profile) and the amplitude of oxygen peak which appears in the survey spectra after the ion treatment. This is an evidence of the dominant mechanism of the ion impact to be the local mechanical decomposition of the polymer structure with further oxygen diffusion through the ion induced defects and its capture by the disturbed fragments. We take the parameter of ξ= O1s/C1s (ratio of 1s oxygen to carbon the integral intensities) as a quantitative measure of the disorder induced into the P3HT film by the implanting ions. We use this parameter to classify the UV-VIS spectra.

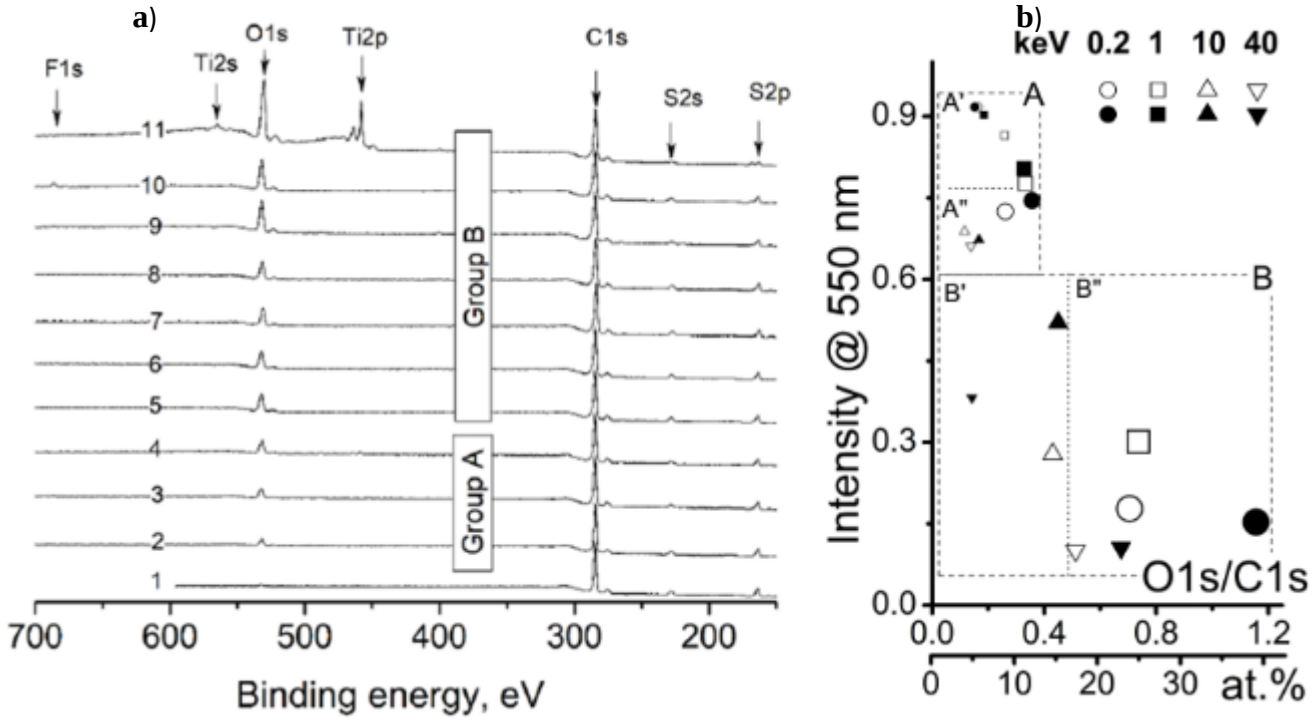

Fig. 4. a) XPS survey spectra of selected samples: 1 – Ref; 2 – F02_13; 3 – F02_14; 4 – Ti02_14; 5 – F10_14; 6 – Ti10_14; 7 – F40_14; 8 – Ti40_14; 9 – F1_15; 10 – F02_15; 11 – Ti02_15.
b) dependence of the UV-VIS absorption intensity at λ =550 nm (from spectra in Fig.3 a) on the ratio of the integral intensities of the XPS peaks of O1s to C1s. A symbol size corresponds to the value of the fluence: 10^{13} cm^{-2} (○●□■▵▲▿▼); 10^{14} cm^{-2} (○●□■▵▲▿▼); 10^{15} cm^{-2}(○ ● □); additional bottom axis represents O1s/C1s in at.%.

Fig. 4b presents the intensity dependence of the reduced absorption spectrum at λ=550 nm on the correspondent ξ value (first replica of the main maximum at around 520 nm). This classification allows us to highlight two distinct transformations of the spectra and to assign them either to group A or B (Fig. 2a). The group A represents spectra with rather slight reduction of the absorption intensity (<0.6), which corresponds to curves 1 – 9 and 12 in Fig. 2a. In particular, this group contains spectra of the samples treated with ions of low energies (0.2 and 1 keV) with low fluencies of 10^{13} and 10^{14} cm^{-2}. The spectra within the A group form two branches (subgroups) A′ and A″. These two branches converge to one point corresponding to $\xi \approx 0.4$ (≈14 at.%), whereas the difference between them increases with ξ decrease below 0.4 (14 at.%). Such a splitting is a result of the principal difference between XPS probing depth restricted within near surface layer and UV-VIS absorption which monitor the integral transformations within the whole bulk of the film. For instance, the beginning of the A″ branch corresponds to 10 keV energy and 10^{13} cm^{-2} fluence, with XPS yielding low ξ values related to just near surface region. Meanwhile the polymer film is disturbed along the stopping path of 31 nm and 19 nm for F^+ and Ti^+ respectively (right axes in Figs. 2 b, c) which relate to curves 8 and 9 in Fig. 2a. A similar behavior is revealed for ions of 40 keV energy and 10^{13} cm^{-2} fluence. However, despite the

projected stopping range of fluorine ions (114 nm) almost twice exceeds that of titanium (56 nm), the titanium ions make stronger impact on the UV-VIS spectrum (curve 13 in Fig. 2a). This means that Ti ions with 40 keV energy cause severe transformations in the polymer film, which is attributed to their big mass (as compared with fluorine) and, hence, momentum sufficient to move an individual nanocrystallite (as discussed in 3.2 paragraph). For this reason, we put this point to the other group B (to B′ subgroup, Fig. 4b). The principal peculiarity of this group is in the character of the spectrum transformations reflecting not only intensity reduction but also spectral modification with the blue shift of the maximum and growth of the short wavelength component. The differences found between A and B groups are similar to those observed in P3HT films during their ageing in two distinct conditions: i) under solar spectrum irradiation in oxygen ambience (A like behavior); ii) in ozone atmosphere in the dark (B like behavior) [31,32]. This suggests that as a consequence of the above discussed scission of the polymer bonds and known ion degradation behavior of P3HT thin films [33] we have to take into account not only shortening of the conjugation chain and decrease of C=C bonds quantity, but also oxidation of P3HT manifested in the appearance of oxygen-containing functional groups. The chemical nature of these groups is not clear yet and to identify it a separate study is needed. However, based on the ratio O1s/C1s in the XPS spectra of the irradiated samples (Table 1), we can assume that their quantity and chemical composition do not depend linearly on energy and fluence of the ions. Moreover, chemical nature of these ions makes different effect only at higher fluences 10^{14} cm^{-2} and 10^{15} cm^{-2} while at lowest fluence 10^{13} cm^{-2} the differences in ξ are minimal in all cases (Table 1). Nevertheless, there is the sharp growth of ξ with fluence and energy of ions in most cases. This fact suggests in turn that the oxidation degree of P3HT significantly increases probably for account of not only grown quantity of oxygen-containing functional groups but also due to the diversity of their nature which can be represented, for example, by hydroxyl, carbonyl, carboxylic and ester groups.

The samples from B″ subgroup are characterized by a complete bleaching which happens after treatments with ions of 40 keV energy and fluence of 10^{14} cm^{-2} or 10^{15} cm^{-2}. Although this result is rather reasonable for 40 keV energy, it is unexpected for lower energies of 0.2 keV or 1 keV with the ion penetrating length much shorter than the film thickness. Eventually, the ion treatment with fluence of 10^{15} cm^{-2} induces at the interface between disturbed and undisturbed regions strong mechanical stresses reduced into strains spreading through the whole depth.

3.4. EPR and NMR

The above results relate to integral characteristics including superposition of various factors. Meantime, our goal is to differentiate between individual mechanisms caused by the ion beam treatment. EPR spectroscopy is a sensitive tool to reveal a selective influence of doping. We use them for the samples with substantial modifications of UV-VIS spectrum as well as dc resistance and ac impedance. The samples after treatments with 10^{14} cm^{-2} fluence are found to be the most characteristic. The spectra of these samples contain lines of three types with g-factors: 2.008; 2.003; within 1.962 – 1.978 range (Fig.5). The line with g=2.003 presents in all the spectra of the above samples. It is found in other reports and attributed to residuals of the polymer synthesis [34] and/or humidity groups [35]. The line with g-factor from the 2.007 – 2.009 range is an evidence of thiolated heterocycles where it is associated with charged $>S^{+\bullet}$ states generated by γ irradiation [36]. We observe this line after the treatment under ion beam regardless of its nature. The line intensity remains the same for the samples irradiated with 10^{14} cm^{-2}fluence (curves 2 – 4 and 5 – 7, Fig.5). Sulfur atoms donate electrons to compensate the positive charge of the implanted ions, which results in the paramagnetic state. Consequently, the intensity of the EPR signal related to this state depends only on the number of implanted species in the polymer film.

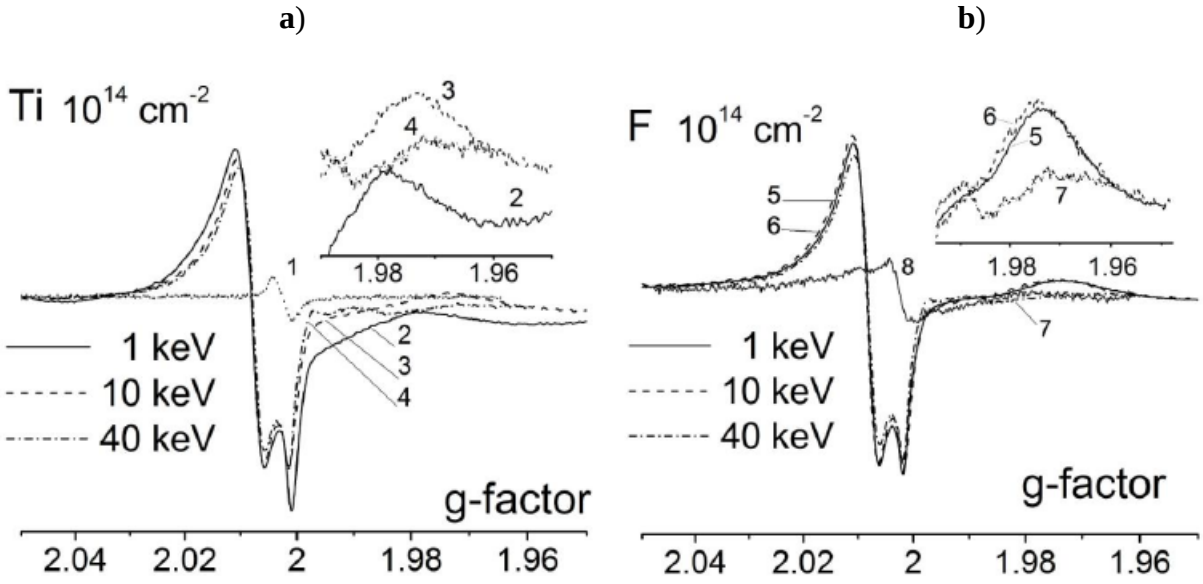

Fig. 5. EPR spectra of the pristine sample (1) and samples treated by correspondent ion beam with 10^{14} cm^{-2} fluence: Ti^+ (a, 2 – 4) and F^+ (b, 5 – 7). 8 – spectrum of F10_15 sample (for comparison). **Insets.** Zoomed-in fragments of the plots.

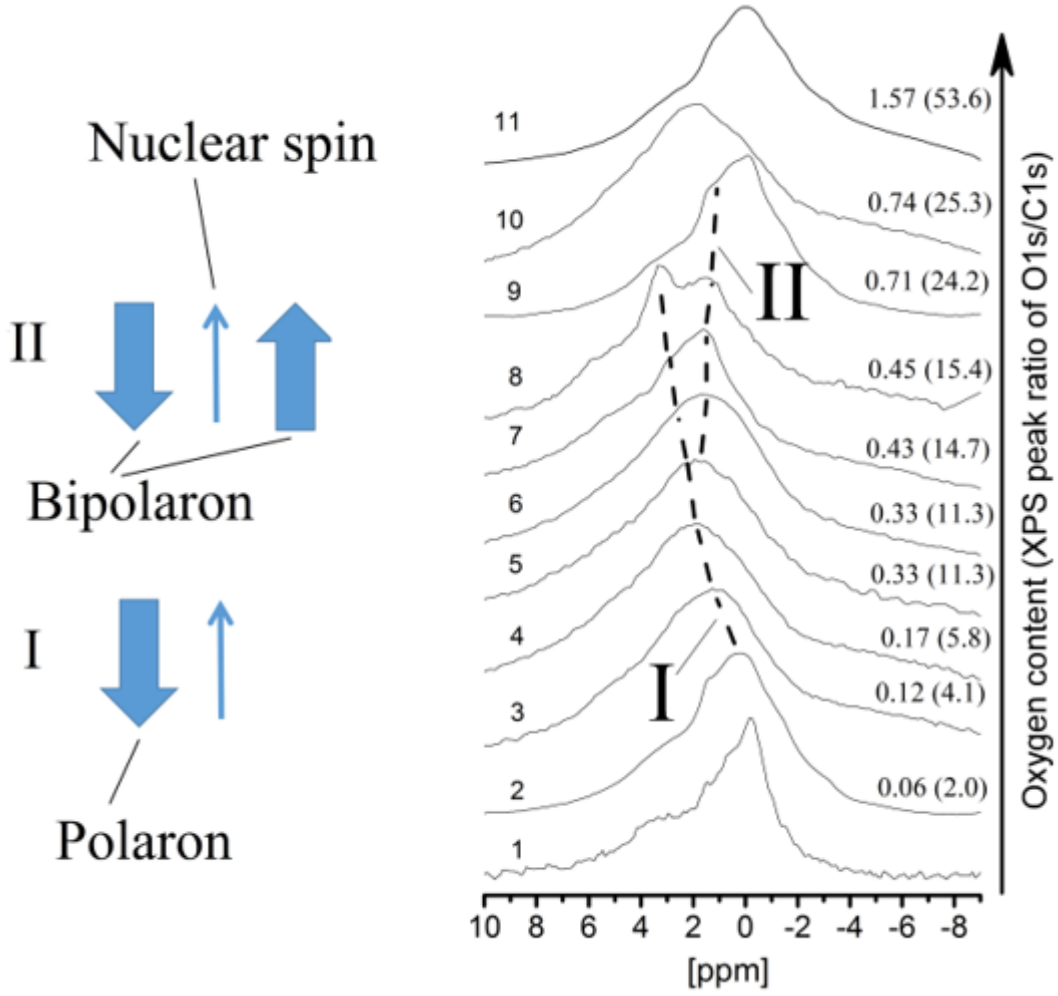

Fig. 6. Right. ^{1}H NMR spectra of: 1 – the glass substrate; 2-11 – rr-P3HT samples: 2 – Ref; 3 – F10_13; 4 – Ti10_13; 5 – Ti1_14; 6 – F1_14; 7 – F10_14; 8 – Ti10_14; 9 – Ti40_14; 10 – F02_15; 11 – F1_15. Figures from the right side are the correspondent values of ξ parameter (with correspondent values in at.% in parentheses). **Left.** Schematic illustration describing the shift: I – downfield shift induced by paramagnetic polaronic state; II – upfield shift as a result of the bipolaronic screening.

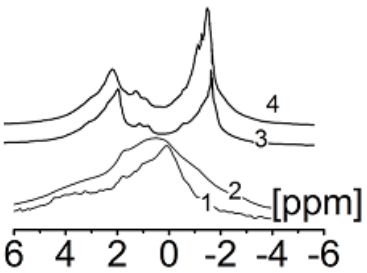

Fig. 7. ^{1}H NMR spectra of the glass substrate (1) and P3HT film spin-coated over the substrate (2 – 4): the pristine P3HT film (2); and after ion implantation at 40 kV, 10^{14} ions/cm^2 with various ions: 3 – fluorine; 4 – titanium.

The components with g<2 are attributed to the localized polaronic paramagnetic state appeared as a result of doping after the ion treatment. Thus, this line can be associated with fragments where polaron is generated at the presence of oxygen known to be a dopant in such a

polymer [37]. The oxygen content increases with energy increase of the implanted ions causing more destructions and higher probability for oxygen diffusion through the ion induced defects [38,39]. However, this line disappears with the energy increase. Nevertheless, this behavior is within doping concept, since the doping level enhancement, in the long run, results in bipolaronic states which are not paramagnetic [40].

^{1}H NMR spectra in Fig. 6 are plotted in the order of the increase of the oxygen content represented by the ξ =O1s/C1s parameter (defined in 3.3 paragraph). The NMR spectra are widened lines (as usually for solid state samples unless magic angle spinning is applied) due to dipole-dipole coupling. Actually, the coupling with the substrate material contributes to the widening as well. The spectrum of the pristine sample (curve 2) follows partially the contour of the glass substrate spectrum (curve 1). As the oxygen content increases the NMR maximum shifts downfield, which is a feature of paramagnetic influence and agrees with the above results on EPR. As ξ reaches 0.33 – 0.43 values (corresponding to 11.3 – 14.7 in at.%) a new component appears in the spectrum. This component shifts in opposite direction with further ξ enhancement, which corresponds to a state where the external field is partially screened. We attribute the latter to the formation of the bipolaronic state. The illustration to this model is depicted in Fig.6 (from the left side).

^{1}H NMR spectra contain characteristic doublet of the molecular hydrogen released after intense collisions of the ions with 40 keV energy and 10^{14} cm^{-2} fluence (Fig. 7, curves 3 and 4). This is the unambiguous evidence of the formation of carbon-rich fragments which have lower resistivity and can also contribute into the overall impedance decrease.

3.5. AFM and DekTak

One of the applicability requirements to the ion implantation for fabrication of organic polymer-based electronic devices is absence of its etching impact on the film. AFM images and data on the thickness measurements confirm the compatibility of the ion implantation with the polymer film (Fig. 8). Surprisingly, there is not only no etching but also there is ~~some~~ a slight increase of its thickness as it follows from DekTak data (Fig. 8d). This is likely attributed to increase of roughness and swelling effect at the surface. It can be observed at the surface after implantation of ions of relatively low energy as the height variation at the surface relief being known to increase with fluence [33]. Our data demonstrate the similar tendency (Fig. 8d): thickness values increase with ξ parameter for each particular case of ion type and energy except for Ti ions with 0.2 keV (non-monotonous with dominant increase) and 10 keV (slightly decreasing).

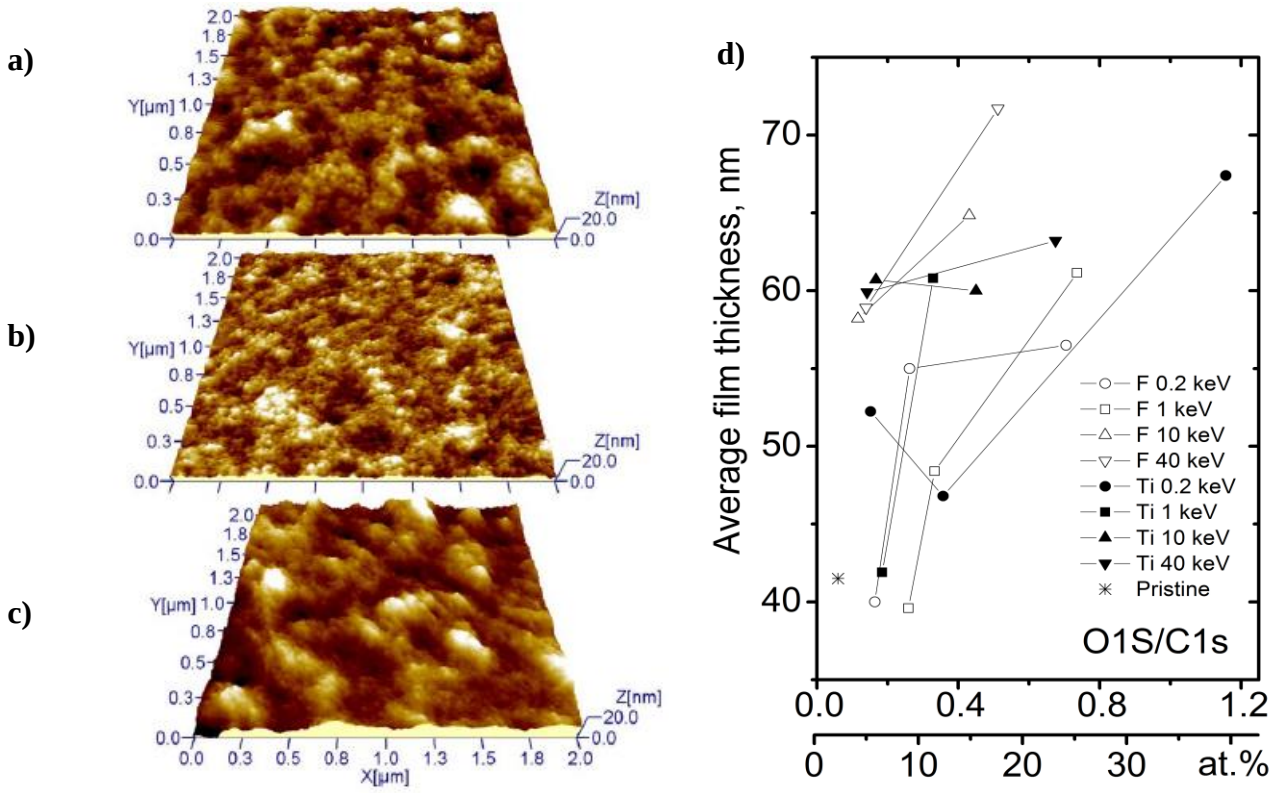

Fig. 8. AFM images (a, b, c) of the samples: a) Ref; b) Ti1_14; c) F1_14. The film thickness (measured by Dektak) versus ξ =O1s/C1s plots (d); additional bottom axis represents O1s/C1s in at.%. A lower value of ξ corresponds to a lower fluence.

Thus, ion beams able to modify the morphology of the film. Although, the detailed study of this phenomenon is beyond the objective of this paper and needs further thorough research.

4. Conclusions

Implantation of fluorine and titanium ions with energies of 0.2 – 40 keV induces in the structure of the rr-P3HT films disturbances causing changes of their properties, such as: i) enhancement of dc resistance after the treatment with high fluence (>10^{14} cm^{-2}); ii) lowering of ac impedance; iii) film bleaching with partial or complete loss of color, which corresponds to the blue shift of the UV-VIS absorption spectra; iv) appearance of new lines in the EPR spectrum with g=2.008 (attributed to the >$S^{+\bullet}$ state ensuring the charge compensation for an implanting ion) and with g<2 (localized polaronic state); v) hydrogen loosening with formation of the molecular hydrogen lines in the ^{1}H NMR spectra after ion implantation with energy 40 keV and 10^{14} cm^{-2} fluence.

In general, the principal outcome of this research consists in compatibility of the low energy ion implantation to the modification of the rr-P3HT films, since this technique does not destroy integrity of the film as a whole and makes no etching, as it follows from AFM images and thickness measurements.

The transformations induced by the ion beams are found to be dominantly associated with (but not restricted by) ion induced defects enabling oxygen infiltration inside the film. The presence of oxygen reflects the extent of the film disturbance which induces local scissoring of chemical bonds with subsequent formation of oxygen-containing functional groups. The signal of O1s XPS is chosen as a quantitative indicator of these disturbances. The more of them, the shorter the average length of the polymer conjugation chain, which determines the blue shift in the UV-VIS absorption spectra. Though the breakage of the conjugation chain hampers the percolation transport contributing to dc resistance of the film, the adjacent fragments used to be parts of the same molecule remain bound via capacitive connection which is evidenced by the decrease of ac impedance. A substantial decrease of the ac impedance after implantation of titanium ions with 40 keV energy and 10^{14} cm^{-2} fluence relates to the formation of carbonized islands (regions with lower content of hydrogen); improvement of the percolation paths between individual nanocrystallites of P3HT after they are shifted by the incident ions; formation of the metallic nanospecies ordered into an alternative percolation net (for the case of titanium ions). The above argues the dominant influence of the titanium ions as compared to fluorine ions. The doping role of oxygen is considered to be one of the constituents relating to the resistance of these films, which envisages the alternative tool for control of the film electrical properties depending on the ambience where samples are placed once removed from the ion implantation chamber.

Acknowledgements

Part of this work has been done at the Ion Beam Center of the Helmholtz-Zentrum Dresden-Rossendorf (HZDR) and financed in part via the BMBF project GUC-LSE (federal research funding of Germany FKZ: 01DK17007) and by the National Academy of Sciences of Ukraine (grant's number #0117U002131). The authors also wish to thank to Dr. Denys Makarov (HZDR) and Prof. Alexander Kordyuk (G. V. Kurdyumov Institute of Metal Physics, NAS of Ukraine) for the fruitful discussions and promotion, to Dr. Tobias Kosub (HZDR) for help with dc resistance measurement set-up and to Prof. Thomas Chases (University of Tuebingen, Tübingen, Baden-Württemberg, Germany) for the useful remarks and constructive comments during the SURFINT-SREN VI meeting.

References

[1] P. R. Berger, M. Kim, Polymer solar cells: P3HT: PCBM and beyond, J. Renewable and Sustainable En. 10 (2018) 013508-1 – 013508-26. https://doi.org/10.1063/1.5012992.

[2] U. Mehmood, A. Al-Ahmed, I.A. Hussein, Review on recent advances in polythiophene based photovoltaic devices, Renewable and Sustainable Energy Reviews 57 (2016) 550 – 561. https://doi.org/10.1016/j.rser.2015.12.177.

[3] S. Agbolaghi, S. Zenoozi, A comprehensive review on poly(3-alkylthiophene)-based crystalline structures, protocols and electronic applications, Organic Electronics 51 (2017) 362 – 403. https://doi.org/10.1016/j.orgel.2017.09.038.

[4] S. A. Gevorgyan, I. M. Heckler, E. Bundgaard, M. Corazza, M. Hösel, R. R. Søndergaard, G.A.R. Benatto, M. Jørgensen , F. C. Krebs, Improving, characterizing and predicting the lifetime of organic photovoltaics: Topical Review, Journal of Physics D: Applied Physics 50 (2017) 103001-1 – 103001-35. https://doi.org/10.1088/1361-6463/50/10/103001.

[5] Shin Hyunji, Park Jaehoon, Baang Sungkeun, Choi Jong Sun, Illumination Effect on Electrical Characteristics of Poly(3-hexylthiophene-2,5-diyl) Thin-Film Transistors, J. Nanosci. and Nanotechnology 20 (2020) 4368 - 4372. https://doi.org/10.1166/jnn.2020.17590.

[6] K. Manoli, P. Seshadri, M. Singh, C. Di Franco, A. Nacci, G. Palazzo, L. Torsia, Solvent-gated Thin-Film-Transistors, Phys. Chem. Chem. Phys. 19 (2017) 20573 - 20581. https://doi.org/10.1039/C7CP03262E.

[7] A.C. Devesh, K. Pathak, M. Tanwar, P. Yogi, P.R. Sagdeo, R. Kumar, Polythiophene–PCBM-Based All-Organic Electrochromic Device: Fast and Flexible, ACS Appl. Electron. Mater. 1 (2019) 58-63. https://doi.org/10.1021/acsaelm.8b00012

[8] Sanyin Qu, Yanling Chen, Wei Shi, Mengdi Wang, Qin Yao, Lidong Chen , Cotton-based wearable poly(3-hexylthiophene) electronic device for thermoelectric application with cross-plane temperature gradient, Thin Sol. Films 667 (2018) 59 – 63. https://doi.org/10.1016/j.tsf.2018.09.046.

[9] C. Enengl, S. Enengl, S. Pluczyk, M. Havlicek, M. Lapkowski, H. Neugebauer, E. Ehrenfreund, Doping- Induced Absorption Bands in P3HT: Polarons and Bipolarons, ChemPhysChem 17 (2016) 3836 – 3844. https://doi.org/10.1002/cphc.201600961.

[10] N. Colaneri, M. Nowak, D. Spiegel, S. Hotta, A.J. Heeger, Bipolarons in poly(3-methylthiophene): Spectroscopic, magnetic, and electrochemical measurements, Phys. Rev. B 36 (1987) 7964 - 7968. https://doi.org/10.1103/PhysRevB.36.7964.

[11] Feili Lai, Yue Wang, Dandan Li, Xianshun Sun, Juan Peng, Xiaodong Zhang, Yupeng Tian,Tianxi Liu, Visible light-driven superoxide generation by conjugated polymers for organic synthesis, Nano Research 11 (2018) 1099 – 1108. https://doi.org/10.1007/s12274-017-1729-6.

[12] T. F. O'Connor, A. V. Zaretski, S. Savagatrup, A. D. Printz, C. D. Wilkes, M. I. Diaz, E. J. Sawyer, D. J. Lipomi, Wearable organic solar cells with high cyclic bending stability: Materials selection criteria, Sol. En. Mater. & Sol. Cells 144 (2016) 438 – 444. http://dx.doi.org/10.1016/j.solmat.2015.09.049.

[13] M. Wang, S. Kee, P. Baek, M.S. Ting, Z. Zujovic, D. Barker, J. Travas-Sejdic, Photo-patternable, stretchable and electrically conductive graft copolymers of poly(3-hexylthiophene), Polymer Chem. 10 (2019) 6278 – 6289. https://doi.org/10.1039/C9PY01428D.

[14] R. Meitzner, T. Faber, S. Alam, A. Amand, R. Roesch, M. Buttner, F. Herrmann-Westendorf, M. Presselt, L. Ciammaruchi, I. Visoly-Fisher, S. Veenstra, A.D. de Zerio, XF Xu, EG Wang, C. Muller, P. Troshin, M.D. Hager, S. Köhn, M. Dusza, M. Krassas, S. Zufle, E. Kymakis, E.A. Katz, S. Berson, F. Granek, M. Manceau, F. Brunetti, G. Polino, U.S. Schubert, M. Lira-Cantu, H. Hoppe, Impact of P3HT materials properties and layer architecture on OPV device stability, Polym. Chem. 10 (2019) 6278 – 6289. https://doi.org/10.1039/C9PY01428D.

[15] B. Lukose, S.V. Bobbili, P. Clancy, Factors affecting tacticity and aggregation of P3HT polymers in P3HT:PCBM blends, Mol. Simulation 43 (2017) 743 – 755. http://dx.doi.org/10.1080/08927022.2017.1303688.

[16] Hyeong Jun Kim, Moo Yeol Lee, Jin-Seong Kim, Jae-Han Kim, Hojeong Yu, Hongseok Yun, Kin Liao, Taek-Soo Kim, Joon Hak Oh, Bumjoon J. Kim, Solution-Assembled Blends of Regioregularity-Controlled Polythiophenes for Coexistence of Mechanical Resilience and Electronic Performance, ACS Appl. Mater. Interfaces 9 (2017) 14120 – 14128. https://doi.org/10.1021/acsami.6b16703.

[17] I.E. Jacobs, A.J. Moule, Controlling Molecular Doping in Organic Semiconductors, Advanced Materials 29 (2017) 1703063-1 – 1703063-39. https://doi.org/10.1002/adma.201703063.

[18] V.V. Kislyuk, O.P. Dimitriev, A.A. Pud, J. Lautru, I. Ledoux-Rak, In-situ conductivity and UV-VIS absorption monitoring of iodine doping-dedoping processes in poly(3-hexylthiophene) (P3HT), Journal of Physics: Conference Series 286 (2011) 012009-1 - 012009-10. doi:10.1088/1742-6596/286/1/012009.

[19] J. Pelletier, A. Anders, Plasma-based ion implantation and deposition: A review of physics, technology, and applications, in IEEE Transactions on Plasma Science 33 (2005) 1944 – 1959. http://escholarship.org/uc/item/84k974r2.

[20] I.H. Loh, R.W. Oliver, P. Sioshansi, Conducting Ploymers by Ion Implantation, Nuclear Instruments and Methods in Physics Research B34 (1988) 337-346. https://doi.org/10.1016/0168-583X(88)90054-7.

[21] M.C. Salvadori, M. Cattani, F.S. Teixeira,I.G. Brown, Conducting polymer formed by low energy gold ion implantation, Applied Physics Letters 93 (2008) 073102-1 – 073102-3. http://dx.doi.org/10.1063/1.2973161.

[22] D.V. Sviridov, Chemical aspects of implantation of high-energy ions into polymeric materials, Russian Chemical Reviews 71 (2002) 315 – 327. https://doi.org/10.1070/RC2002v071n04ABEH000710.

[23] V.N. Popok, Ion Implantation of Polymers: Formation of nanopartuculate Materials, Rev.Adv.Mater. Sci. 30 (2012) 1 – 26.

[24] D. Brenes-Badilla, D. J. Coutinho, D. R. B. Amorim, R. M. Faria, and M. C. Salvadori, Reversing an S-kink effect caused by interface degradation in organic solar cells through gold ion implantation in the PEDOT:PSS layer, J. Appl. Phys. 123 (2018) 155502-1 – 155502-6. https://doi.org/10.1063/1.5017672.

[25] K. Yoshino, S. Hayashi, K. Kaneto, J. Okube, T. Moriya, T. Matsuyama, H. Yamaoka, Radiation Effect in Conducting Polymers, Mol. Crystals and Liquid Crystals 121 (1985) 255 – 258. https://doi.org/10.1080/00268948508074871.

[26] N.M. Isa, R. Baharin, R.A. Majid, W.A.W.A. Rahman, Optical properties of conjugated polymer: review of its change mechanism for ionizing radiation sensor, Polym. Adv. Technol. 28 (2017) 1559 – 1571. https://doi.org/10.1002/pat.4067

[27] U. Salzner, J.B. Lagowski, P.G. Pickup, R.A. Poirier, Comparison of geometries and electronic structures of polyacetylene, polyborole, polycyclopentadiene, polypyrrole, polyfuran, polysilole, polyphosphole, polythiophene, polyselenophene and polytellurophene, Synthetic Metals 96 (1998) 177-189. https://doi.org/10.1016/S0379-6779(98)00084-8.

[28] Takashi Nishino, Takuya Matsumoto, Atsunori Mori, Alternative Aspects of Polythiophenes, in: New Polymeric Materials Based on Element-Blocks, Y. Chujo (ed.), Springer, Nature, Singapore Pte Ltd., 2019, pp. 153 – 165. https://doi.org/10.1007/978-981-13-2889-3_9

[29] H. Matsuoka, S. Mizutani, C. Watanabe, S. Yamauchi, High-Frequency EPR Studies on Polymer Chain Morphology in Dip-Coated Films of Poly(3-hexylthiophene)/Fullerene Bulk-Heterojunctions, Bull. Chem. Soc. Jpn. 89 (2016) 378–384. doi:10.1246/bcsj.20150400.

[30] Hidetaka Konno, X-ray Photoelectron Spectroscopy, in: Materials Science and Engineering of Carbon, ed. by Michio Inagaki, Elsevier, 2016.

[31] M. Manceau, J. Gaume, A. Rivaton, J.-L. Gardette, G. Monier, L. Bideux, Further insights into the photodegradation of poly(3-hexylthiophene) by means of X-ray photoelectron spectroscopy, Thin Solid Films 518 (2010) 7113 – 7118. https://doi.org/10.1016/j.tsf.2010.06.042.

[32] H. Hintz, H.-J. Egelhaaf, H. Peisert, T. Chassé, Photo-oxidation and ozonization of poly(3-hexylthiophene) thin films as studied by UV/VIS and photoelectron spectroscopy, Polymer

Degradation and Stability 95 (2010) 818 – 825. https://doi.org/10.1016/j.polymdegradstab.2010.02.004

[33] M. Sezen, H. Plank, P.M. Nellen, S. Meier, B. Chernev, W. Grogger, E. Fisslthaler, E.J.W. List, U. Scherf, P. Poelt, Ion beam degradation analysis of poly(3-hexylthiophene) (P3HT): can cryo-FIB minimize irradiation damage?, Phys. Chem. Chem. Phys. 11, (2009) 5130–5133. https://doi.org/10.1039/B816893H

[34] A. Sperlich, H. Kraus, C. Deibel, H. Blok, J. Schmidt, V. Dyakonov, Reversible and Irreversible Interactions of Poly(3-hexylthiophene) with Oxygen Studied by Spin-Sensitive Methods, J. Phys. Chem. B 115 (2011) 13513 – 13518. https://doi.org/10.1021/jp2077215.

[35] R. Bauld, L.M. Fleury, M. Van Walsh, G. Fanchini, Correlation between density of paramagnetic centers and photovoltaic degradation in polythiophene-fullerene bulk heterojunction solar cells, Appl. Phys. Lett. 101 (2012), 103306-1 – 103306-4. http://dx.doi.org/10.1063/1.4749813.

[36] G. Strzelczak, E. Janeba-Bartoszewicz, I. Carmichael, B. Marciniak, K. Bobrowski, Electron paramagnetic resonance (EPR) study of γ-radiation-induced radicals in 1,3,5-trithiane and its derivatives, Res. on Chemical Intermediates 35 (2009) 507 – 517. https://doi.org/10.1007/s11164-009-0054-4.

[37] H. Hintz, H. Peisert, H.-J. Egelhaaf, T. Chassé, Reversible and Irreversible Light-Induced p-Doping of P3HT by Oxygen Studied by Photoelectron Spectroscopy (XPS/UPS), Phys. Chem. C 115 (2011) 13373 – 13376. https://doi.org/10.1021/jp2032737

[38] Z.J. Han, B.K. Tay, P.C.T. Ha, M.Shakerzadeh, A.A.Cimmino, S.Prawer, D. McKenzie, Electronic conductance of ion implanted and plasma modified polymers, Appl. Phys. Lett. 91 (2007) 052103-1 – 052103-3. https://doi.org/10.1063/1.2761233.

[39] D. Fink, R. Klett, Latent Ion Tracks in Polymers for Future Use in Nanoelectronics: an Overview of the Present State-of-the-Art, Brazilian Journal of Physics 25 (1995) 54 – 75.

[40] F. Devreux, F. Genoud, M. Nechtschein, B. Villeret, ESR investigation of polarons and bipolarons in conducting polymers: the case of polypyrrole, Synthetic Metals 18 (1987) 89-94. https://doi.org/10.1016/0379-6779(87)90859-9.

Figure captions

Fig. 1. The sample resistance measured from 4-probe circuit versus fluence of the respective ion beam. **Inset.** Photo of a sample with contacts. The contact numbers correspond to the following connections: 1,2 – power supply; 3,4 – voltmeter (top view).

Fig.2. a) UV-VIS absorption spectra of the rr-P3HT samples: 1 – Ref, F02_13, Ti02_13; 2 – Ti1_13; 3 – F1_13; 4 – Ti1_14; 5 – F1_14; 6 – Ti02_14; 7 – F02_14; 8 – F10_13; 9 – Ti10_13; 10 – Ti10_14; 11 – F10_14; 12 – F40_13; 13 – Ti40_13; 14 – F40_14; 15 – Ti40_14; 16 – F1_15; 17 – F02_15; 18 – Ti02_15. b,c) dependencies which relate ion energy in keV, the stopping range projection R_p in nm (calculated in SRIM software) and ratio of the 1s XPS peak intensities of oxygen and carbon O1s/C1s for samples treated by ions of F (b) and Ti (c) for two values of fluence: 10^{13} cm^{-2} (△,▲) and 10^{14} cm^{-2} (□,■); additional bottom axes represent O1s/C1s in at.%.

Fig. 3. a), b), c): Nyquist diagrams plotted on the basis of ac impedance spectroscopy data; **d)** schematic representation of the equivalent circuit for the fragment subjected to the ion beam: I – before and II – after the ion incidence.

Fig. 4. a) XPS survey spectra of selected samples: 1 – Ref; 2 – F02_13; 3 – F02_14; 4 – Ti02_14; 5 – F10_14; 6 – Ti10_14; 7 – F40_14; 8 – Ti40_14; 9 – F1_15; 10 – F02_15; 11 – Ti02_15.

b) dependence of the UV-VIS absorption intensity at λ =550 nm (from spectra in fig.3 a) on the ratio of the integral intensities of the XPS peaks of O1s to C1s. A symbol size corresponds to the value of the fluence: 10^{13} cm^{-2} (○●□■△▲▽▼); 10^{14} cm^{-2} (○●□■△▲▽▼); 10^{15} cm^{-2}(○●□); additional bottom axis represents O1s/C1s in at.%.

Fig. 5. EPR spectra of the pristine sample (1) and samples treated by correspondent ion beam with 10^{14} cm^{-2} fluence: Ti^+ (a, 2 – 4) and F^+ (b, 5 – 7). 8 – spectrum of F10_15 sample (for comparison). **Insets.** Zoomed-in fragments of the plots.

Fig. 6. Right. ^{1}H NMR spectra of: 1 – the glass substrate; 2-11 – rr-P3HT samples: 2 – Ref; 3 – F10_13; 4 – Ti10_13; 5 – Ti1_14; 6 – F1_14; 7 – F10_14; 8 – Ti10_14; 9 – Ti40_14; 10 – F02_15; 11 – F1_15. Figures from the right side are the correspondent values of ξ parameter (with correspondent values in at.% in parentheses). **Left.** Schematic illustration describing the shift: I – downfield shift induced by paramagnetic polaronic state; II – upfield shift as a result of the bipolaronic screening

Fig. 7. ^{1}H NMR spectra of the glass substrate (1) and P3HT film spin-coated over the substrate (2 – 4): the pristine P3HT film (2); and after ion implantation at 40 kV, 10^{14} ions/cm^2 with various ions: 3 – fluorine; 4 – titanium.

Fig. 8. AFM images (a, b, c) of the samples: a) Ref; b) Ti1_14; c) F1_14. The film thickness (measured by Dektak) versus ξ =O1s/C1s plots (d); additional bottom axis represents O1s/C1s in at.%. A lower value of ξ corresponds to a lower fluence.

Credit Author Statement

Victor Kislyuk: Conceptualization, Data Curation, Writing - Original Draft, Writing - Review & Editing, Visualization, Supervision
Sergiy Kotrechko: Methodology, Writing - Original Draft, Writing - Review & Editing, Supervision
Volodymyr Trachevskij: Validation, Investigation, Resources, Writing - Original Draft, Writing - Review & Editing
Andrii Melnyk: Formal analysis, Investigation, Data Curation
Alexander Pud: Methodology, Resources, Writing - Original Draft, Writing - Review & Editing, Supervision
Nikolay Ogurtsov: Investigation, Resources
Yuriy Noskov: Investigation, Resources
Mykola Osiponok: Resources
Peter Lytvyn: Investigation, Resources, Data Curation
Yulia Dzyazko: Investigation, Resources
Shavkat Akhmadaliev: Validation, Formal analysis, Software
Ulrich Kentsch: Validation, Formal analysis, Investigation, Resources, Supervision
Matthias Krause: Investigation, Validation, Resources, Supervision
Stefan Facsko: Validation, Formal analysis, Data Curation, Writing - Original Draft, Writing - Review & Editing, Supervision, Project administration

Figure 1

Click here to access/download;Figure;Fig 1.jpg

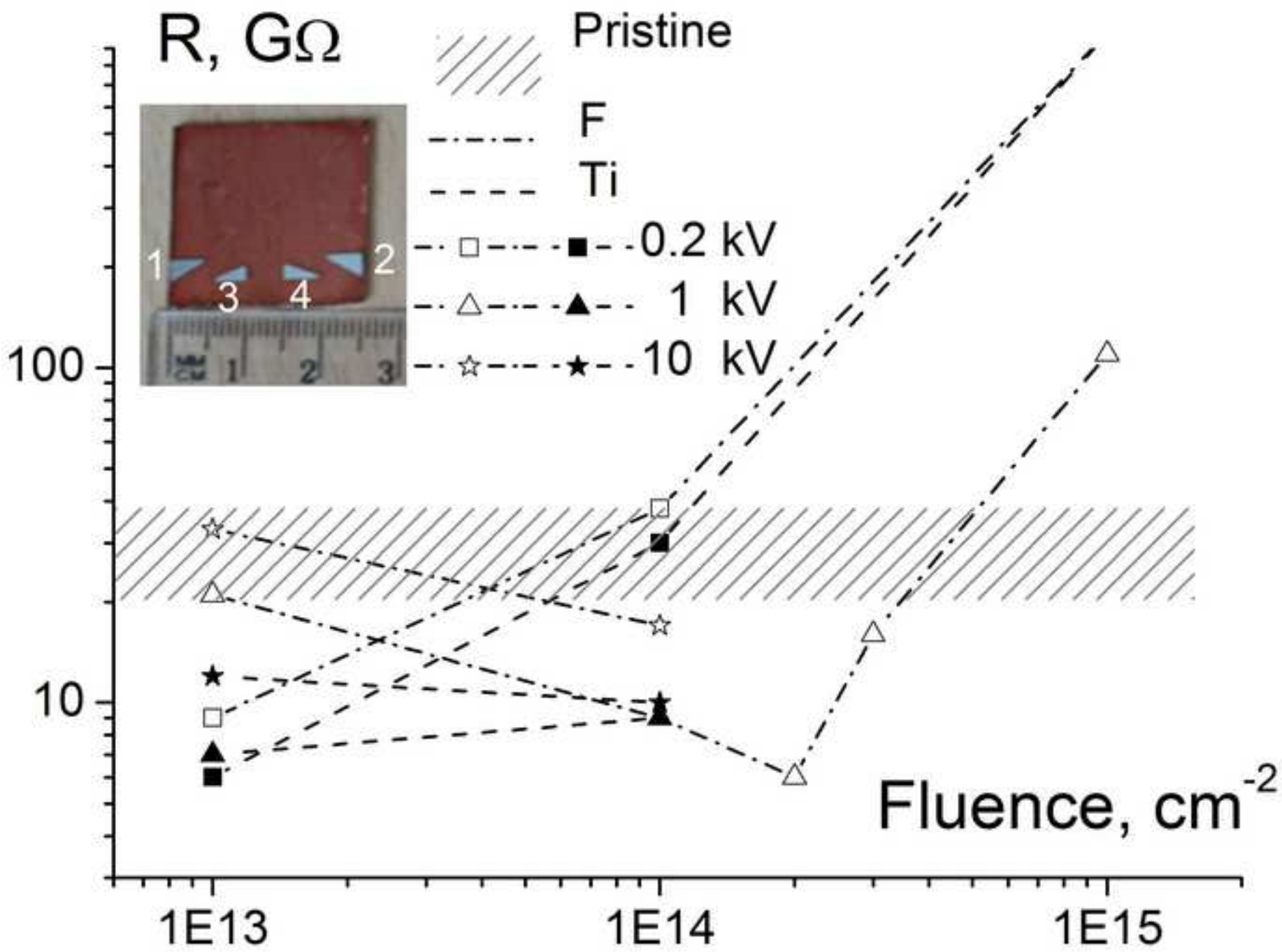

Figure 2a

Click here to access/download;Figure;Fig 2a.jpg

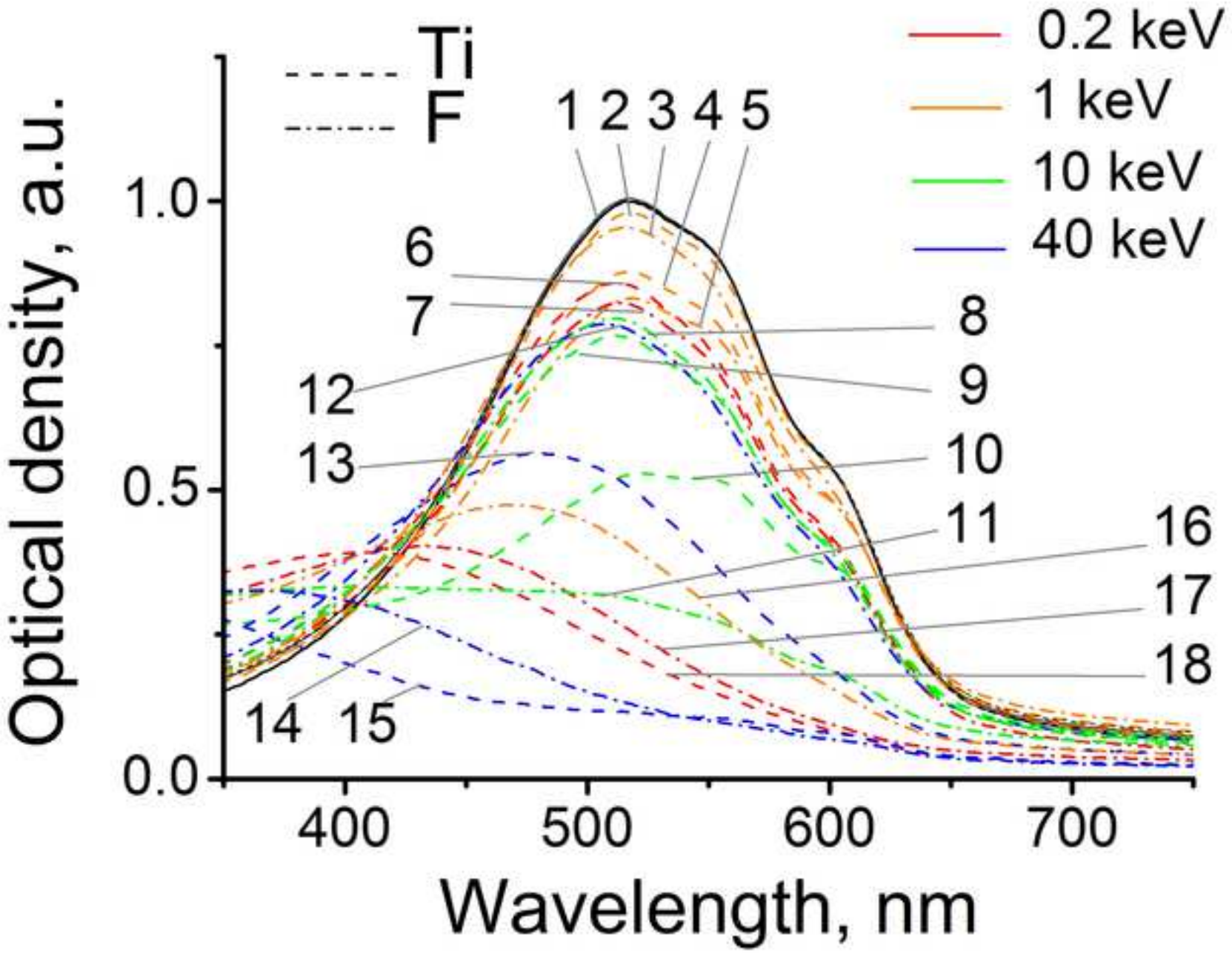

Figure 2b

Click here to access/download;Figure;Fig 2b.jpg

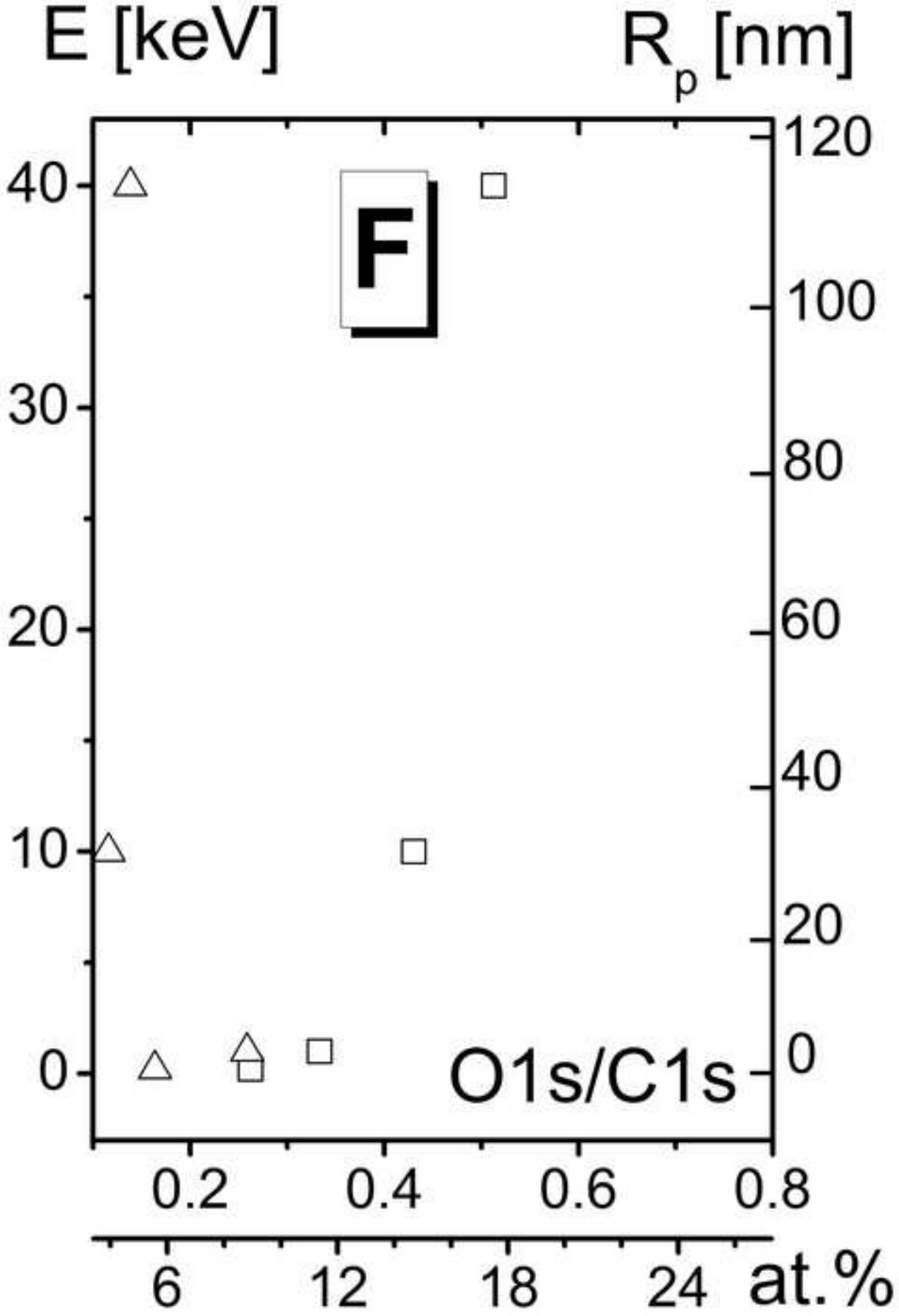

Figure 2c

Click here to access/download;Figure;Fig 2c.jpg

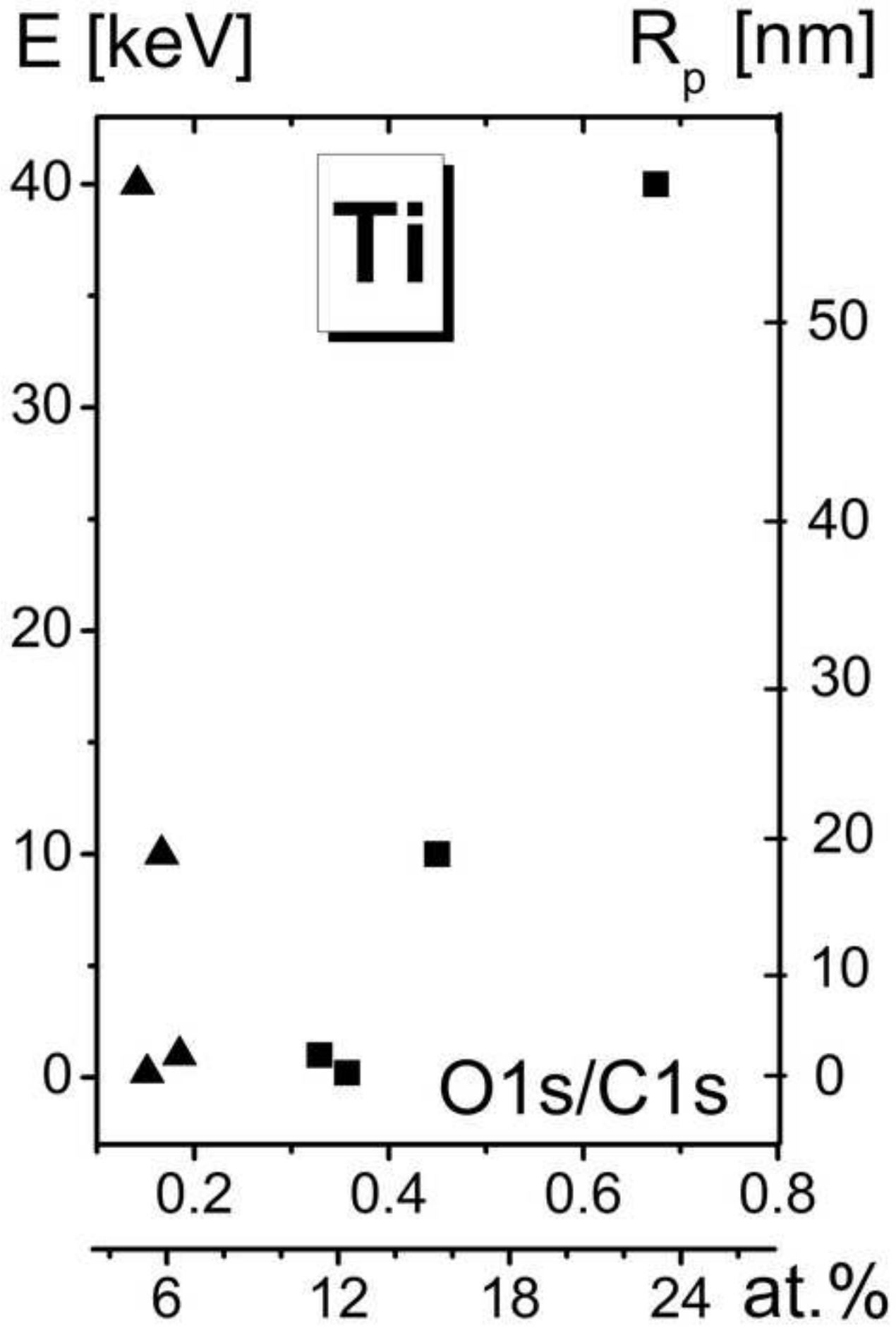

Figure 3a

Click here to access/download;Figure;Fig 3a.jpg

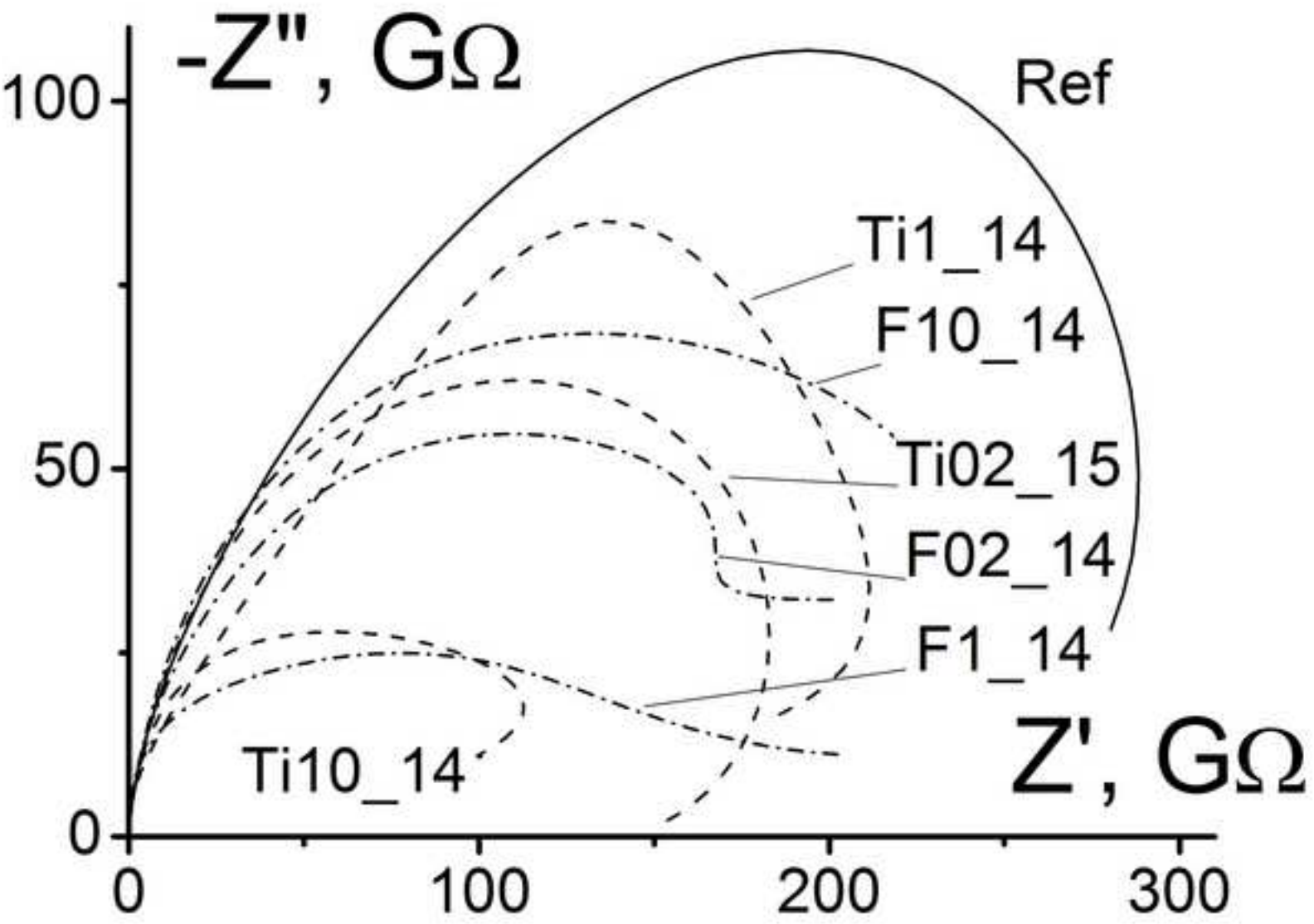

Figure 3b

Click here to access/download;Figure;Fig 3b.jpg

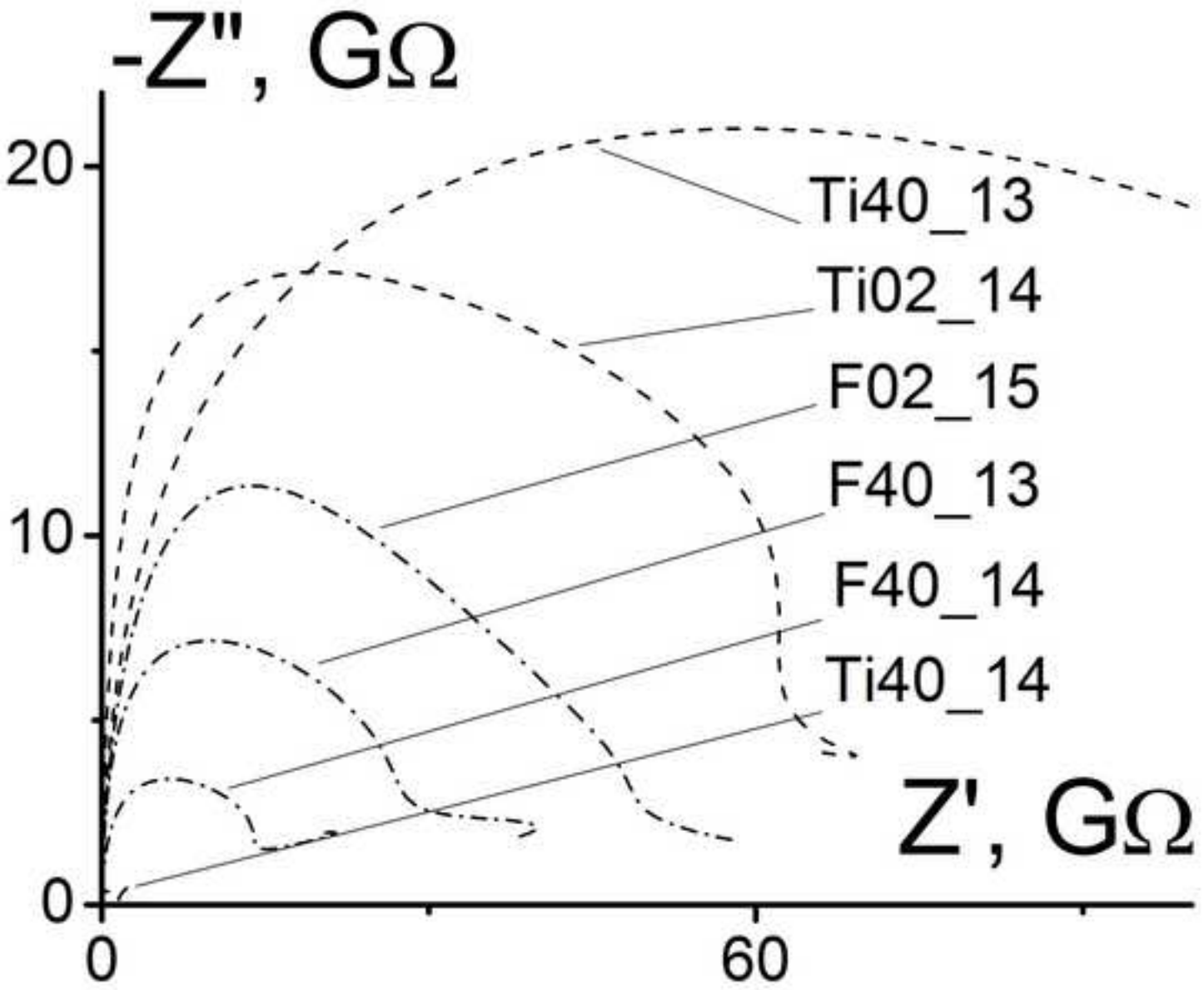

Figure 3c

Click here to access/download;Figure;Fig 3c.jpg

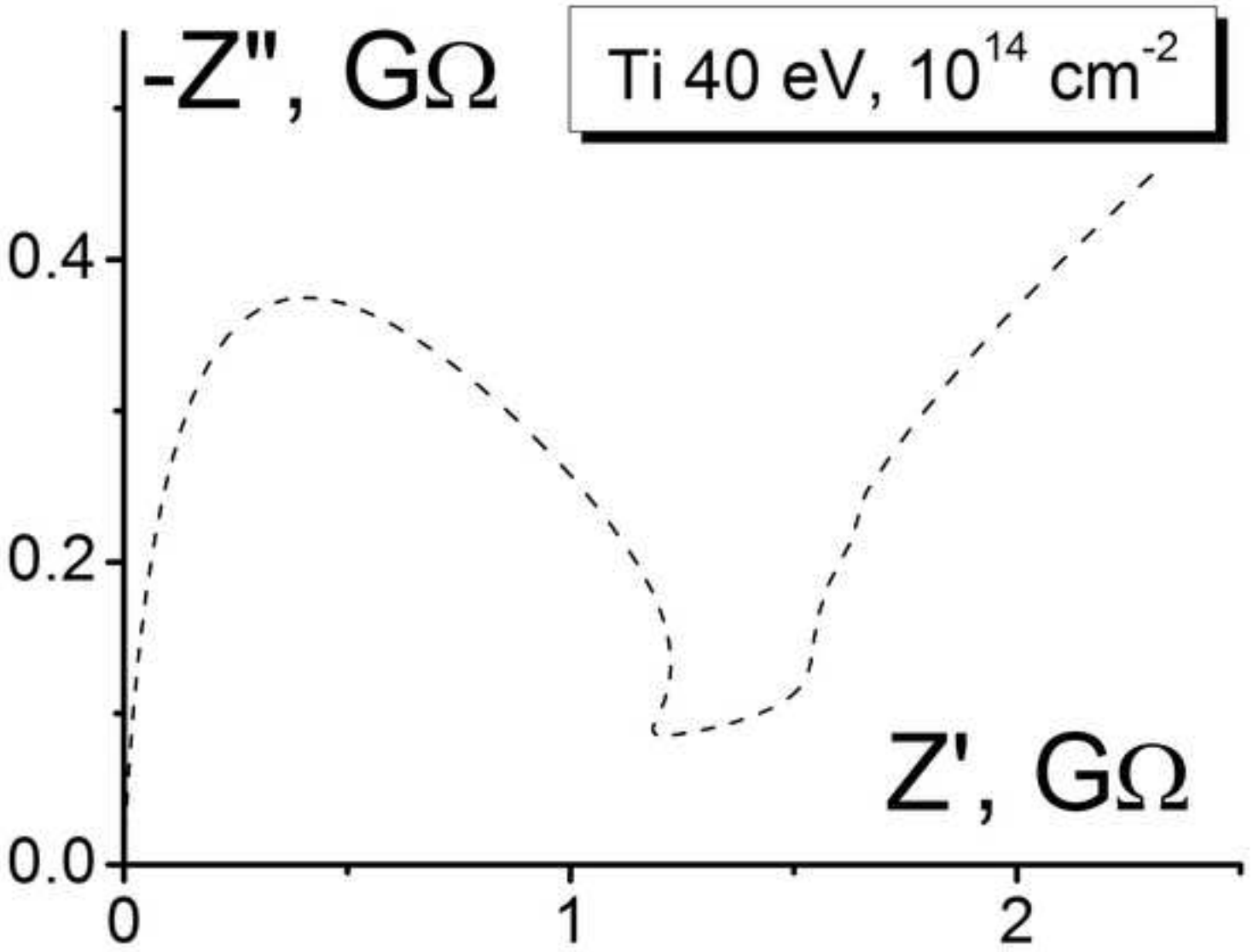

Figure 3d

Click here to access/download;Figure;Fig 3d.jpg

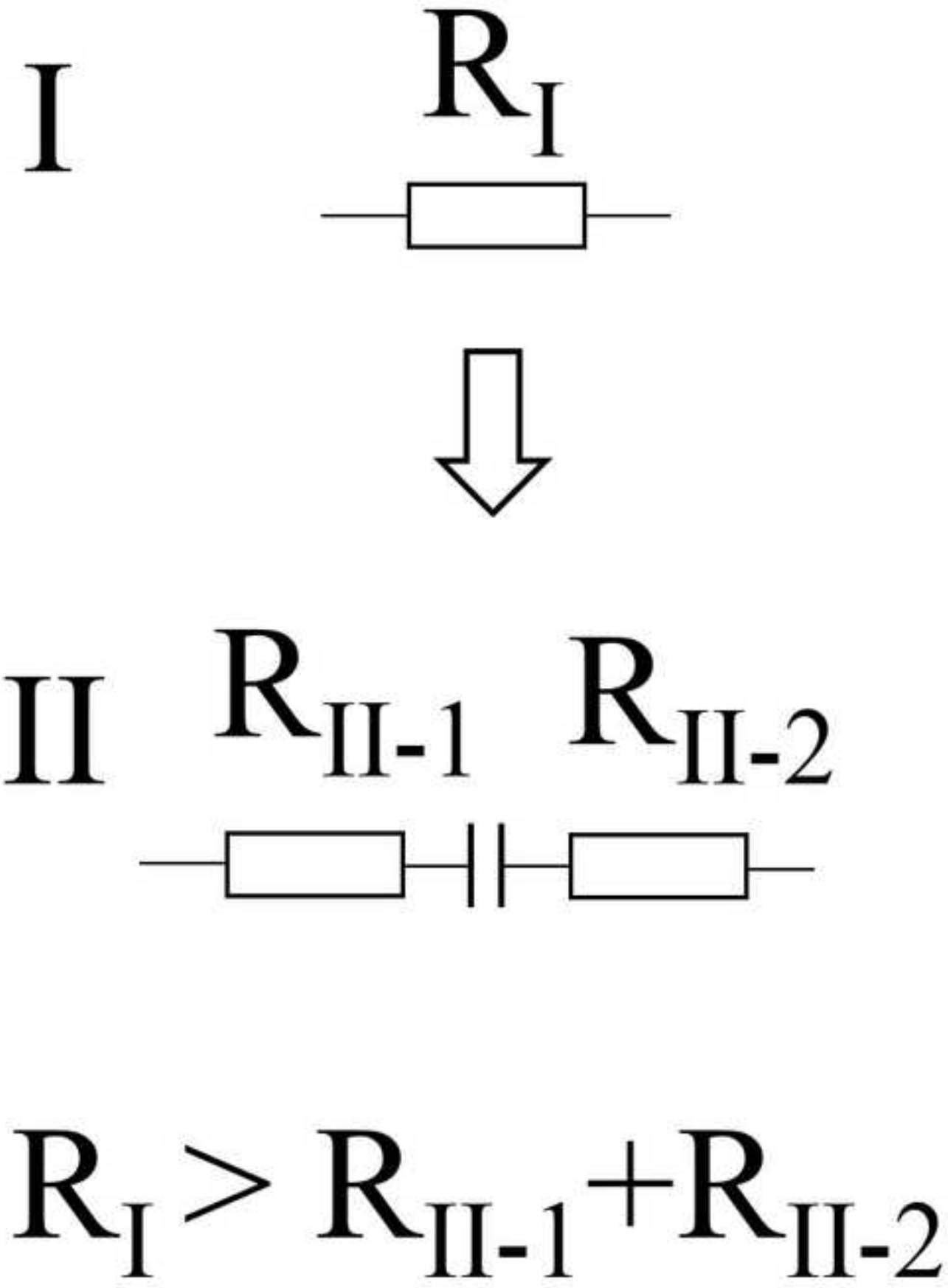

Figure 4a

Click here to access/download;Figure;Fig 4a.jpg

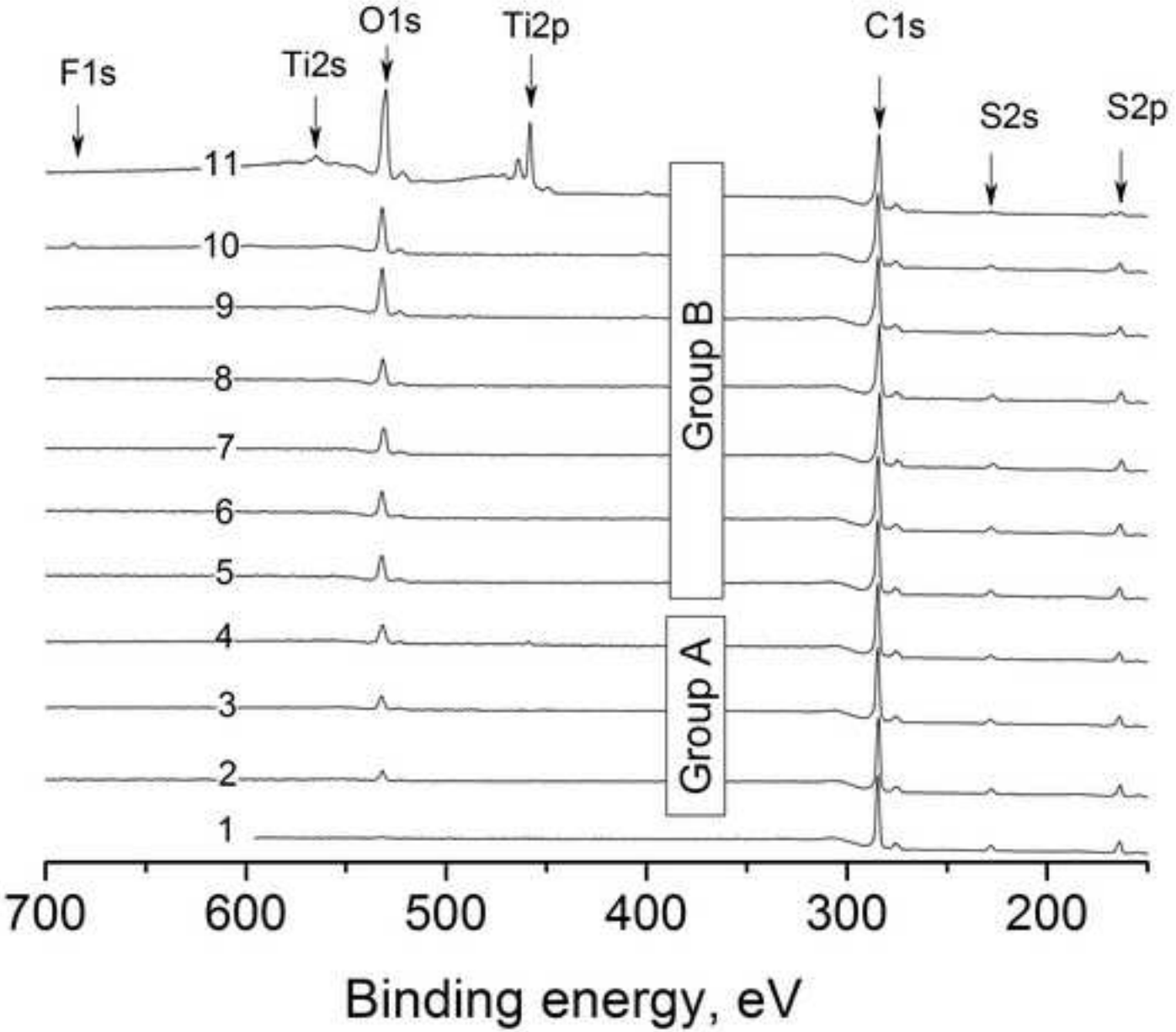

Figure 4b

Click here to access/download;Figure;Fig 4b.jpg

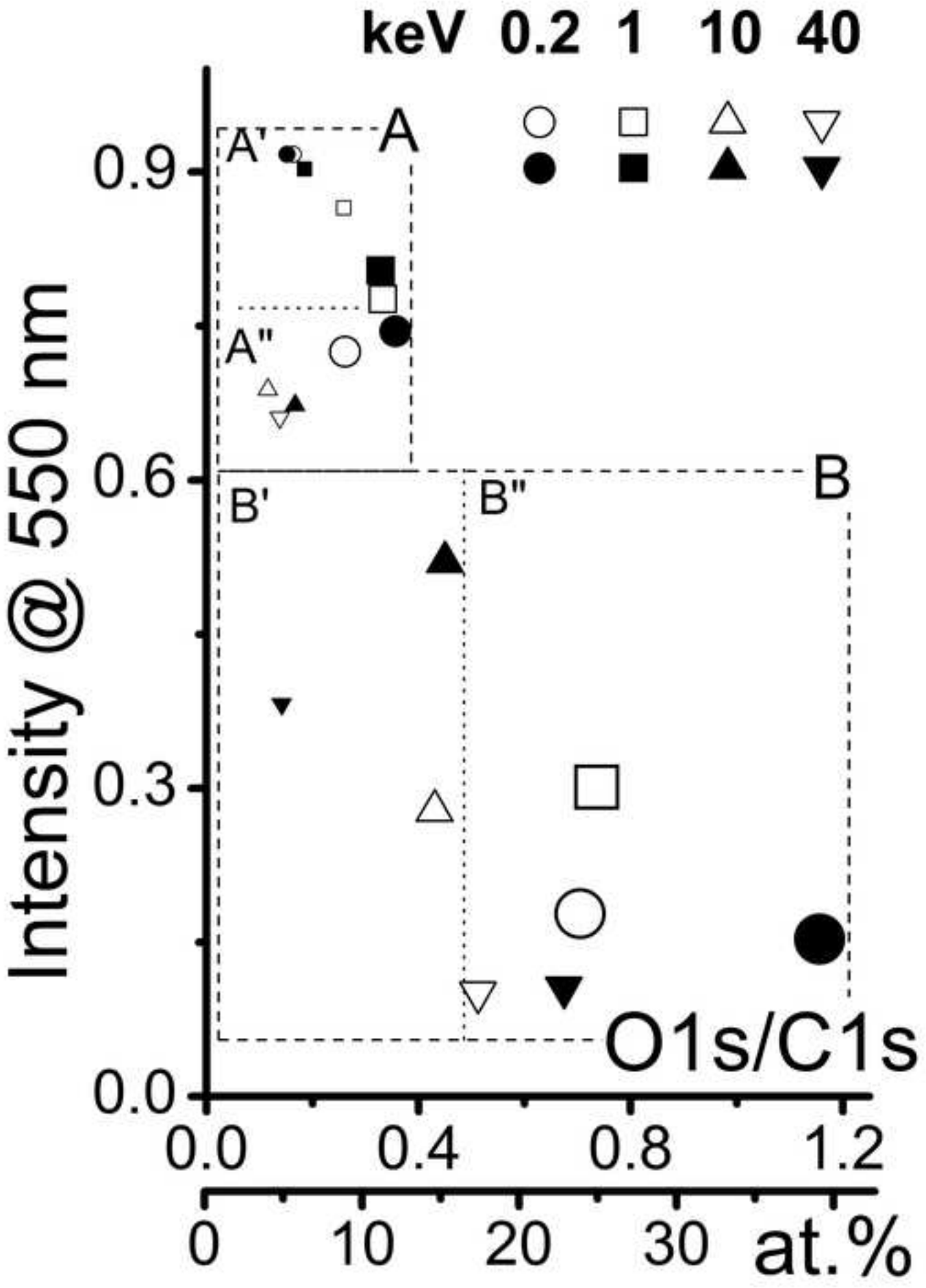

Figure 5a

Click here to access/download;Figure;Fig 5a.jpg

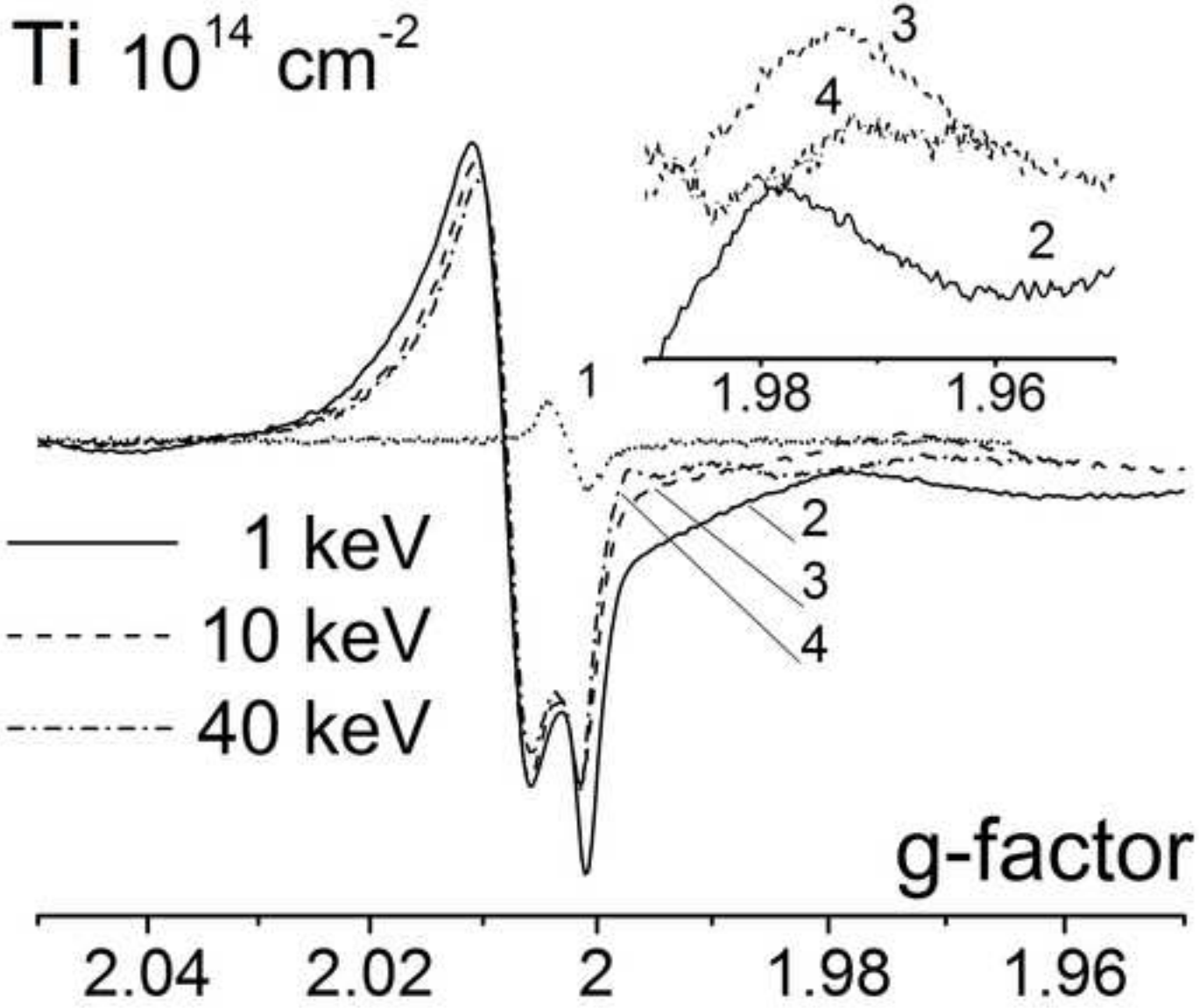

Figure 5b

Click here to access/download;Figure;Fig 5b.jpg

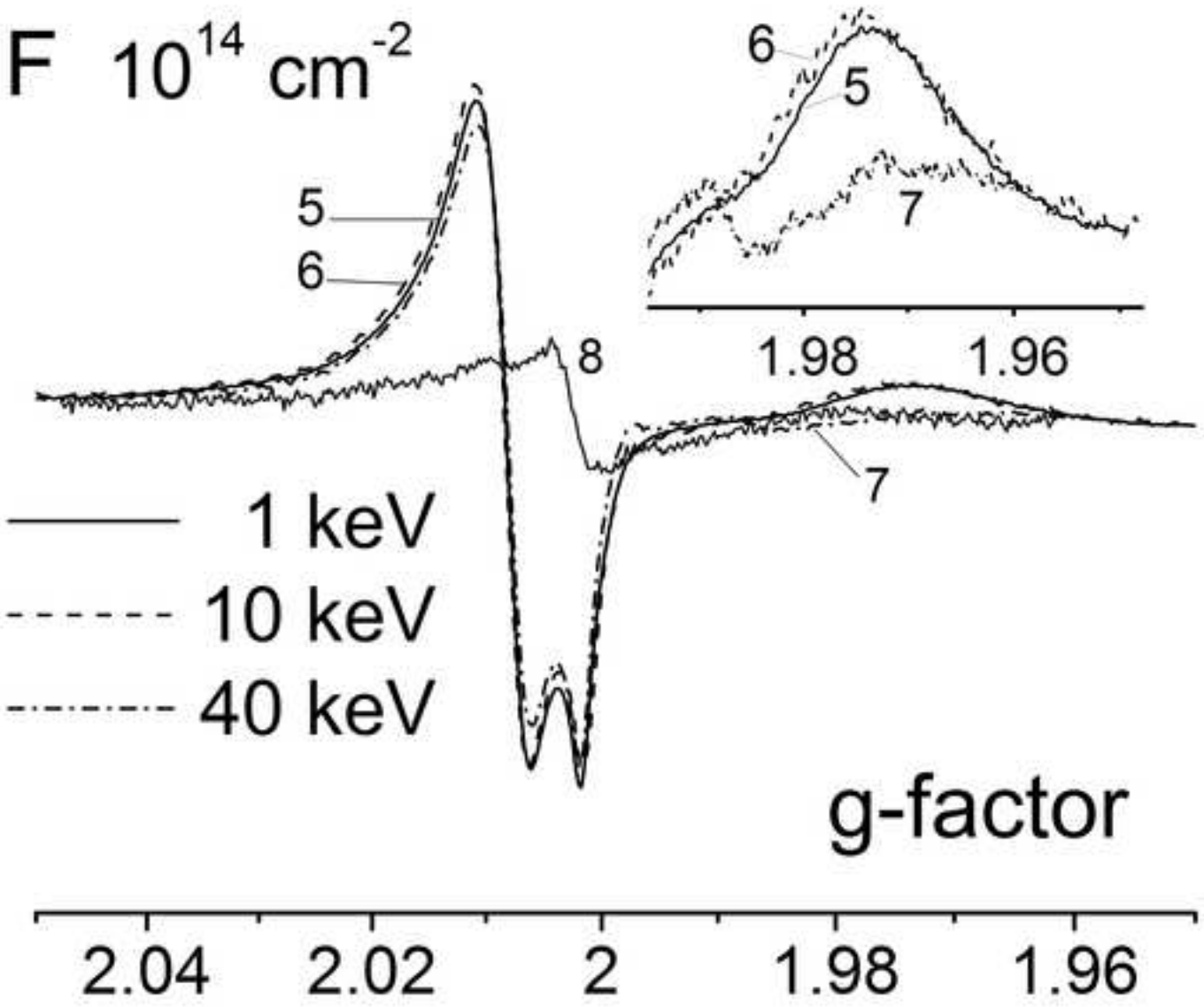

Figure 6

Click here to access/download;Figure;Fig 6.jpg

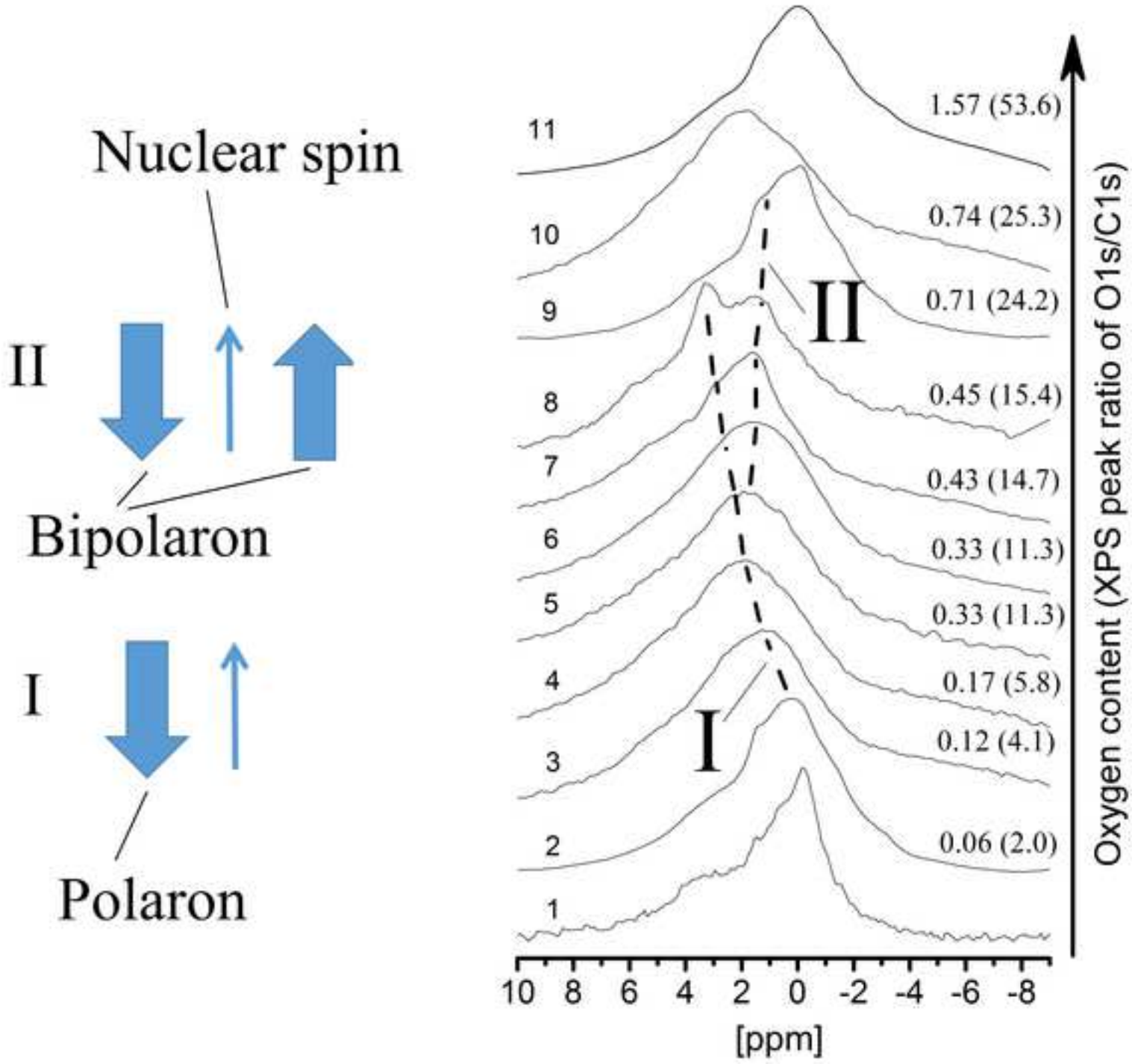

Figure 7

Click here to access/download;Figure;Fig 7.jpg

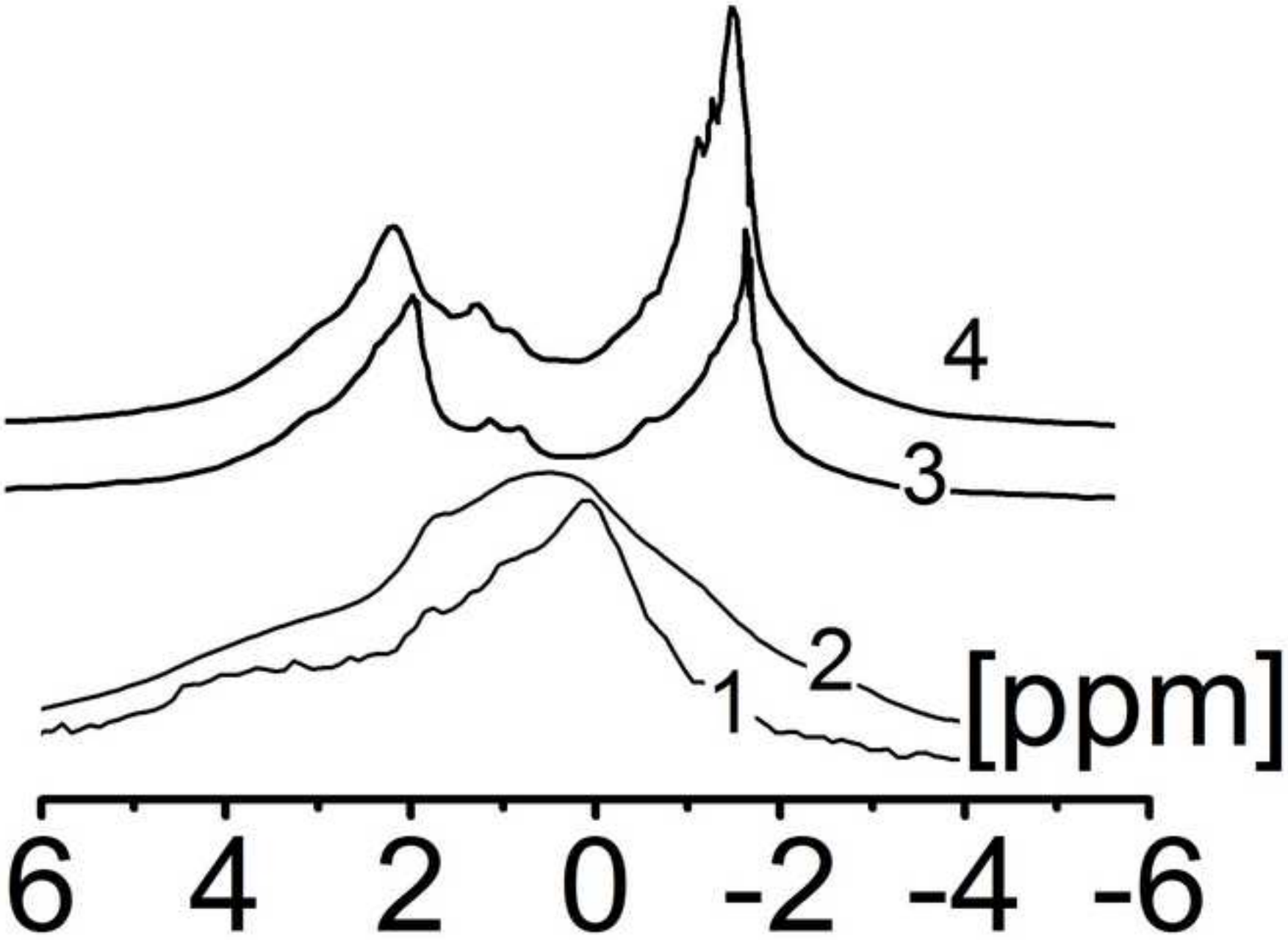

Figure 8abc

Click here to access/download;Figure;Fig 8abc.jpg

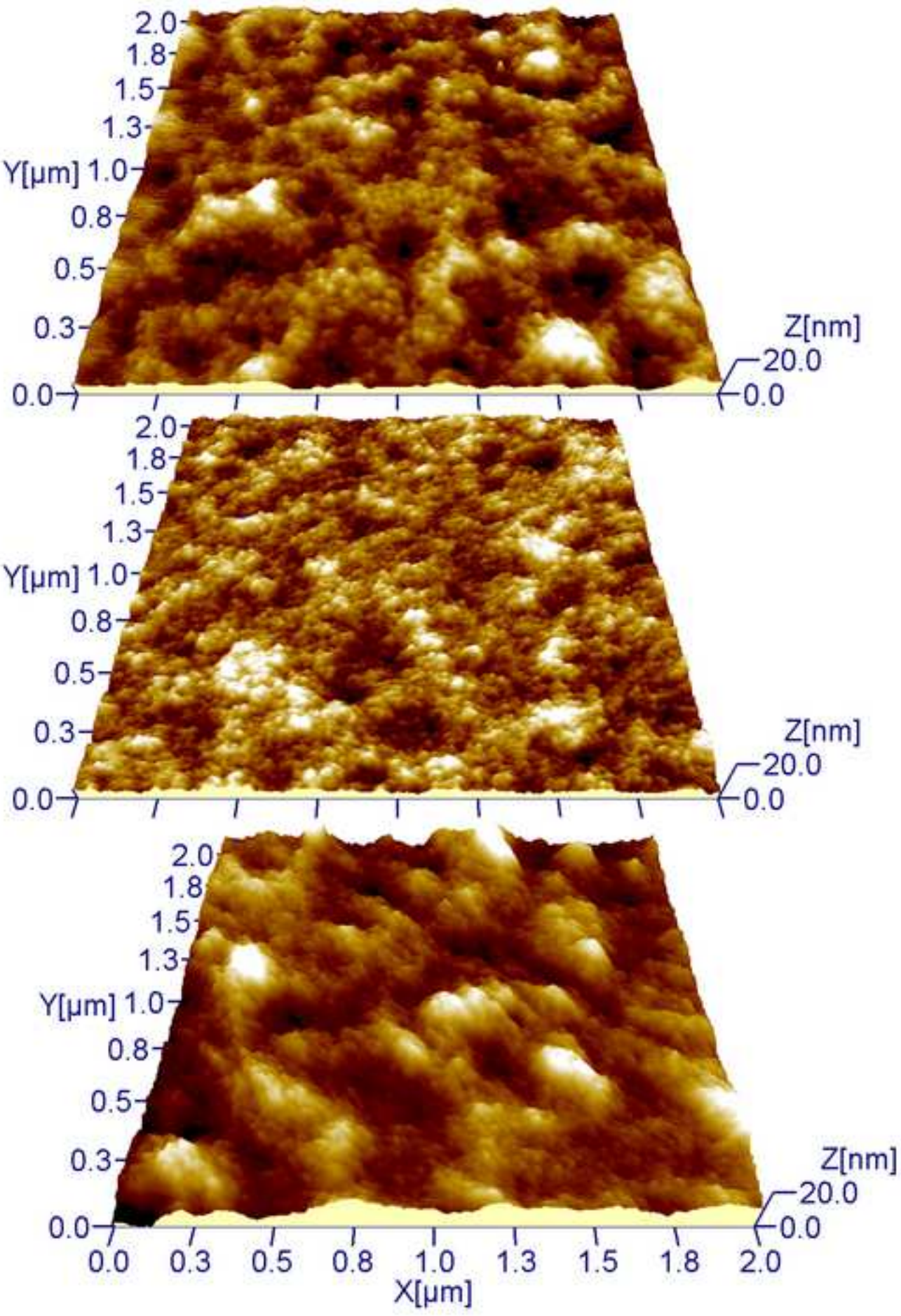

Figure 8d

Click here to access/download;Figure;Fig 8d.jpg

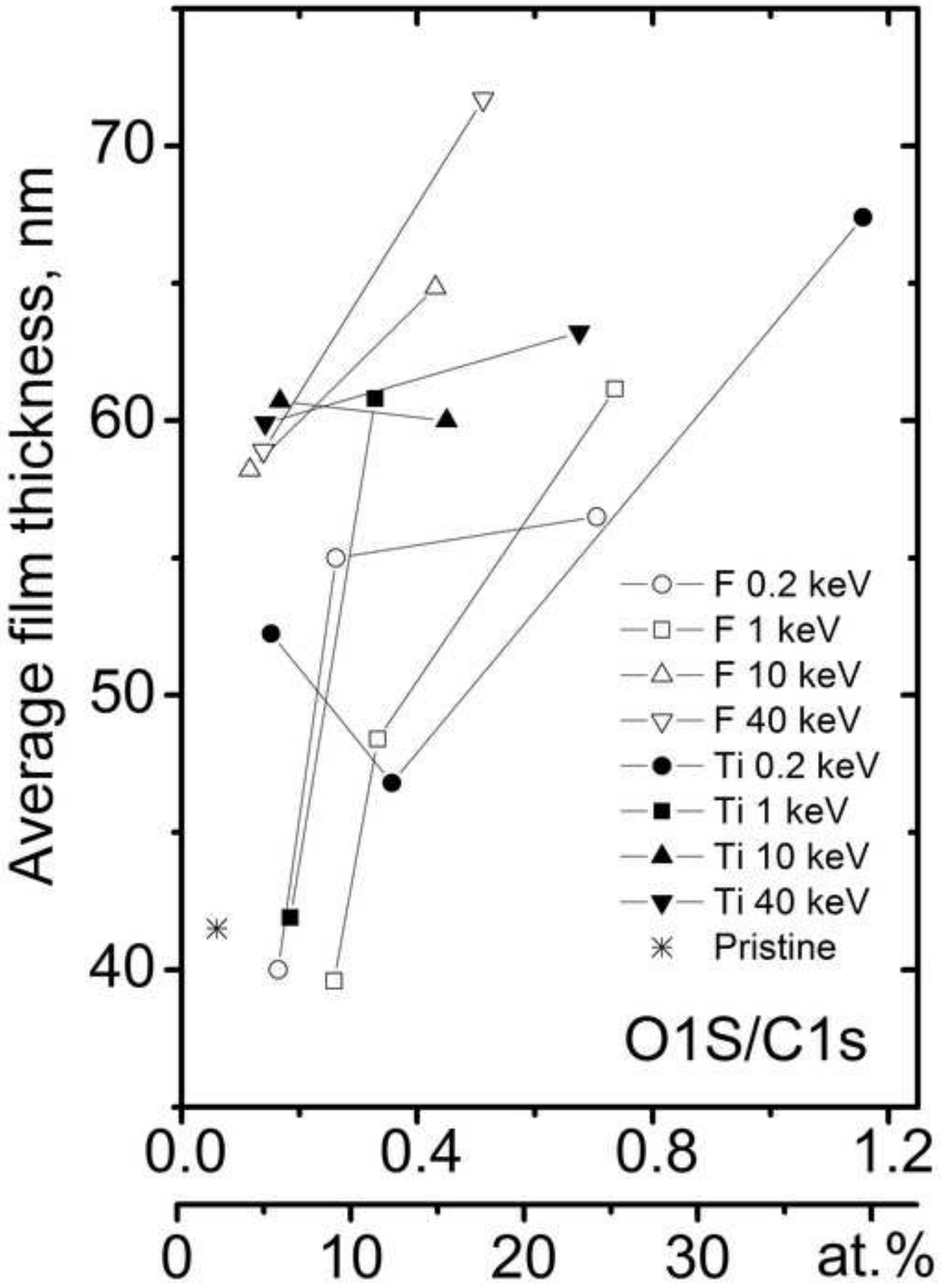

Table

Table 1. The sample list with description of the ion beam treatment. Parameters of ξ =O1s/C1s, $\xi_{at} = \xi \cdot S_{C1s}/S_{O1s}$, where O1s, C1s, S_{C1s}/S_{O1s} =1/2.93 are intensities of XPS signals for 1s electrons of oxygen and carbon and ratio of their R.S.F., respectively.

No.	Sample code	Ion type	Energy, eV	Fluence, cm^{-2}	ξ	ξ_{at}, %
1	Ref	Pristine sample	-	-	0.06	2.0
2	F02_13	F^+	0.2	10^{13}	0.16	5.5
3	F02_14	F^+	0.2	10^{14}	0.26	8.9
4	F02_15	F^+	0.2	10^{15}	0.71	24.2
5	F1_13	F^+	1	10^{13}	0.26	8.9
6	F1_14	F^+	1	10^{14}	0.33	11.3
7	F1_15	F^+	1	10^{15}	0.74	25.3
8	F10_13	F^+	10	10^{13}	0.12	4.1
9	F10_14	F^+	10	10^{14}	0.43	14.7
10	F10_15	F^+	10	10^{15}	-	-
11	F40_13	F^+	40	10^{13}	0.14	4.8
12	F40_14	F^+	40	10^{14}	0.51	17.4
13	Ti02_13	Ti^+	0.2	10^{13}	0.15	5.1
14	Ti02_14	Ti^+	0.2	10^{14}	0.36	12.3
15	Ti02_15	Ti^+	0.2	10^{15}	1.57	53.6
16	Ti1_13	Ti^+	1	10^{13}	0.18	6.1
17	Ti1_14	Ti^+	1	10^{14}	0.33	11.3
18	Ti10_13	Ti^+	10	10^{13}	0.17	5.8
19	Ti10_14	Ti^+	10	10^{14}	0.45	15.4
20	Ti40_13	Ti^+	40	10^{13}	0.14	4.8
21	Ti40_14	Ti^+	40	10^{14}	0.67	22.9